

  
**MITSUBISHI HEAVY INDUSTRIES, LTD.**

16-5, KONAN 2-CHOME, MINATO-KU

TOKYO, JAPAN

January 16, 2009

Document Control Desk  
U.S. Nuclear Regulatory Commission  
Washington, DC 20555-0001

Attention: Mr. Jeffrey A. Ciocco

Docket No. 52-021  
MHI Ref: UAP-HF-09002

**Subject: MHI's Partial Responses to the NRC's Requests for Additional Information on Topical Report MUAP-07013-P (R0) "Small Break LOCA Methodology for US-APWR"**

**Reference:** 1) "REQUEST FOR ADDITIONAL INFORMATION ON TOPICAL REPORT MUAP-07013-P, 'SMALL BREAK LOCA METHODOLOGY FOR US-APWR'," dated December 2, 2008.

With this letter, Mitsubishi Heavy Industries, Ltd. ("MHI") transmits to the U.S. Nuclear Regulatory Commission ("NRC") an official document entitled "MHI's Partial Responses to the NRC's Requests for Additional Information on Topical Report MUAP-07013-P (R0) 'Small Break LOCA Methodology for US-APWR'". In the enclosed document, MHI provides the 68 (sixty-eight) out of 80 (eighty) items requested in Reference 1. The remaining responses to the RAI in Reference 1 will be transmitted to the NRC by separate correspondence, no later than February 16, 2009 (75 days after the issuance of the formal RAI), as agreed by NRC and MHI.

As indicated in the enclosed materials, this document contains information that MHI considers proprietary, and therefore should be withheld from public disclosure pursuant to 10 C.F.R. § 2.390 (a)(4) as trade secrets and commercial or financial information which is privileged or confidential. A non-proprietary version of the document is also being submitted in this package (Enclosure 3). Any proprietary information that is written inside a bracket in the proprietary-version is replaced by the designation "[ ]" without any text, in the non-proprietary-version.

This letter includes a copy of proprietary version (Enclosure 2), a copy of non-proprietary version (Enclosure 3), and the Affidavit of Yoshiki Ogata (Enclosure 1) which identifies the bases of MHI request that all materials designated as "Proprietary" in Enclosure 2 be withheld from public disclosure pursuant to 10 C.F.R. § 2.390 (a)(4).

Please contact Dr. C. Keith Paulson, Senior Technical Manager, Mitsubishi Nuclear Energy Systems, Inc. if the NRC has questions concerning any aspect of this submittal. His contact information is provided below.

Sincerely,



Yoshiki Ogata  
General Manager - APWR Promoting Department  
Mitsubishi Heavy Industries, LTD.

DOB  
NRD

Enclosures:

1. Affidavit of Yoshiki Ogata
2. MHI's Partial Responses to the NRC's Requests for Additional Information on Topical Report MUAP-07013-P (R0) "Small Break LOCA Methodology for US-APWR" (proprietary)
3. MHI's Partial Responses to the NRC's Requests for Additional Information on Topical Report MUAP-07013-P (R0) "Small Break LOCA Methodology for US-APWR" (non-proprietary)

CC: J. A. Ciocco  
C. K. Paulson

Contact Information

C. Keith Paulson, Senior Technical Manager  
Mitsubishi Nuclear Energy Systems, Inc.  
300 Oxford Drive, Suite 301  
Monroeville, PA 15146  
E-mail: ck\_paulson@mnes-us.com  
Telephone: (412) 373 – 6466

## ENCLOSURE 1

Docket No.52-021  
MHI Ref: UAP-HF-09002

### MITSUBISHI HEAVY INDUSTRIES, LTD.

#### AFFIDAVIT

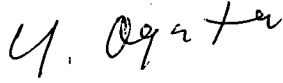
I, Yoshiki Ogata, being duly sworn according to law, depose and state as follows:

1. I am General Manager, APWR Promoting Department, of Mitsubishi Heavy Industries, Ltd ("MHI"), and have been delegated the function of reviewing MHI's US-APWR documentation to determine whether it contains information that should be withheld from disclosure pursuant to 10 C.F.R. § 2.390 (a)(4) as trade secrets and commercial or financial information which is privileged or confidential.
2. In accordance with my responsibilities, I have reviewed the enclosed "MHI's Partial Responses to the NRC's Requests for Additional Information on Topical Report MUAP-07013-P (R0) 'Small Break LOCA Methodology for US-APWR'" and have determined that portions of the report contain proprietary information that should be withheld from public disclosure. Those pages containing proprietary information are identified with the label "Proprietary" on the top of the page and the proprietary information has been bracketed with an open and closed bracket as shown here "[ ]". The first page of the technical report indicates that all information identified as "Proprietary" should be withheld from public disclosure pursuant to 10 C.F.R. § 2.390 (a)(4).
3. The information in the report identified as proprietary by MHI has in the past been, and will continue to be, held in confidence by MHI and its disclosure outside the company is limited to regulatory bodies, customers and potential customers, and their agents, suppliers, and licensees, and others with a legitimate need for the information, and is always subject to suitable measures to protect it from unauthorized use or disclosure.
4. The basis for holding the referenced information confidential is that it describes the unique codes and files developed by MHI for the fuel of the US-APWR and also contains information provided to MHI under license from the Japanese Government. These codes and files were developed at significant cost to MHI, since they required the performance of detailed calculations, analyses, and testing extending over several years. The referenced information is not available in public sources and could not be gathered readily from other publicly available information. MHI knows of no way the information could be lawfully acquired by organizations or individuals outside of MHI and the Japanese Government.
5. The referenced information is being furnished to the Nuclear Regulatory Commission ("NRC") in confidence and solely for the purpose of supporting the NRC staff's review of MHI's Application for certification of its US-APWR Standard Plant Design.
6. Public disclosure of the referenced information would assist competitors of MHI in their design of new nuclear power plants without the costs or risks associated with the design of new fuel systems and components. Disclosure of the information identified as

proprietary would therefore have negative impacts on the competitive position of MHI in the U.S. nuclear plant market.

I declare under penalty of perjury that the foregoing affidavit and the matters stated therein are true and correct to the best of my knowledge, information and belief.

Executed on this 16<sup>th</sup> day of January, 2009.

A handwritten signature in black ink, appearing to read "Y. Ogata". The signature is written in a cursive style with a large initial "Y" and a long horizontal stroke at the end.

Yoshiki Ogata  
General Manager- APWR Promoting Department  
Mitsubishi Heavy Industries, LTD.

Enclosure 3

UAP-HF-09002

**MHI's Partial Responses to the NRC's Requests for Additional  
Information on Topical Report MUAP-07013-P (R0)  
"Small Break LOCA Methodology for US-APWR"**

January 2009  
(Non-Proprietary)

## INTRODUCTION

This document presents MHI's partial responses to the NRC's requests for additional information (RAI) on Topical Report MUAP-07013-P (R0) "Small Break LOCA Methodology for US-APWR" dated December 2, 2008.

This document provides the 68 items requested in this RAI. The remaining responses will be transmitted to the NRC by separate correspondence, no later than February 16, 2009.

## **REQUEST 1-1**

Table 1.1-1

The table attempts to present the correspondence between the organization of the SBLOCA methodology topical report (MUAP-07013-P (R0)) and the roadmap identified in Regulatory Guide 1.203 for the development and assessment of the evaluation methodology. Different sections of the topical report are associated with the 20 steps identified in the Regulatory Guide. Provide a more refined association of sub-sections of the topical report to the 20 steps. For example, Section 8 is identified to address Step 15: Assess Scalability of Models. However, there is no specific section title in Section 8 that addresses the task identified in Section 15.

## **RESPONSE**

Reviewer is correct. MHI has missed to provide an individual section for Step 15 (Assessment of Models Scalability). However, it is already implicitly discussed in Section 5 (Step 6) entitled "Perform Scaling Analysis and Identify Similarity Criteria". Therefore, MHI now summarizes the scaling analysis results from each test (IET, SET) and conclude them.

The scalability of the experimental facilities used for the validation of the code is well verified. Therefore, the physical model is also applicable for the plant analysis including for the US-APWR. To reflect the sequence of steps in EM development and assessment based on the RG 1.203, the following modification has been made:

**Section 8.1: Input Preparation and Calculations to Assess Model Fidelity or Accuracy (Step 14)** - *The content is the same.*

**Section 8.2: Models Scalability Assessment (Step 15)** → new section to be created.  
- *The content is the summary of those reported in Section 5 about Scaling Analysis and Similarity Criteria Identification, and the Identification of existing data of the Integral Effects Tests (IETs) and Separate Effect Tests (SETs) to complete the Database.*

**Section 8.3: Determining the Capability of Field Equations to Represent Process and Phenomena and the Ability of Numeric Solutions to Approximate Equation Set (Step 16)**  
- *The content is the same.*

**Section 8.4: Determining the Applicability of Evaluation Model to Simulate System Components (Step 17)**  
- *The content is the same*

**Section 8.5: Input Preparation and Calculations to Assess System Interactions and Global Capability (Step 18)**  
- *This section was previously designated as Section 8.2, the content remains the same.*

### **Draft of the new Section 8.2:**

#### **8.2 Models Scalability Assessment**

The scalability evaluation is limited to whether the specific model or correlation is appropriate for application to the configuration and conditions of the plant and transient under evaluation. The scaling issue was basically resolved in Step 6. This section provides the summary and conclusion.

To validate the M-RELAP5 code for the high-ranking phenomena, six (6) Separate Effect Tests (SETs) and one (1) Integral Effects Test (IET) are selected as follows:

1. ROSA/LSTF Void Profile test
2. ORNL/THTF Void Profile test
3. ORNL/THTF Uncovered heat transfer test
4. ORNL/THTF Reflood test
5. UPTF SG plenum CCFL test
6. Dukler Air-Water Flooding test
7. ROSA-IV/LSTF small break (5%) LOCA test (SB-CL-18)

The scalability of the above tests to the US-APWR model is described in the following subsections:

### **8.2.1 Separate Effect Tests (SETs)**

#### **8.2.1.1 Scalability of the ROSA/LSTF Void Profile Test**

- Elevations: preserved, i.e., one-to-one correspondence with the reference PWR. Because the LSTF hot and cold leg inner diameters (IDs) are smaller than those of the reference PWR, only the elevations of the top of the primary hot and cold legs were set equal to those of the reference PWR.
- Volumes: scaled by the facility scaling factor 1/48.
- Flow area: scaled by 1/48 in the pressure vessel and 1/24 in the steam generators. However, the hot and cold legs were scaled to conserve the ratio of the length to the square root of pipe diameter, i.e.,  $L/\sqrt{D}$  for the reference PWR. Such an approach was adopted to better simulate the flow regime transition in the primary loops.
- Core power: scaled by 1/48 at core powers equal to or less than 14% of the scaled reference PWR rated power. The LSTF rated and steady-state power is 10 MWt, i.e., 14% of the rated reference PWR core power scaled by 1/48. With this scaled core power, a reduced core inlet flow rate can be obtained and the condition of the steam generator secondary side is changed to accommodate the scaled power.
- Fuel assembly: dimensions, i.e., fuel rod diameter, pitch and length, guide thimble diameter pitch and length, and ratio of number of fuel rods to number of guide thimbles, designed to be the same as the 17x17 fuel assembly of the reference PWR to preserve the heat transfer characteristics of the core. The total number of rods 1064 for heated rods and 104 for unheated rods. They are scaled by 1/48.
- Design pressures: approximately the same as the reference PWR.
- Fluid flow differential pressures ( $\Delta P$ s): set to be equal to the reference PWR for scaled flow rates.
- Flow capacities: scaled by the overall scaling factor where practicable.
- Core and lower plenum: in comparison with the reference PWR, the length of the heated zone, fuel rod diameter and pitch, power peaking factor and number of spacers are conserved. The core volume and the number of fuel rods are scaled at a ratio of 1/48.

#### **8.2.1.2 Scalability of the ORNL/THTF Void Profile Test**

Thermal Hydraulic Test Facility (THTF) contains a 64-rod electrically heated bundle with internal dimensions typical of a 17x17 PWR fuel assembly. The scaling of the facility is acceptable because it adopts full length and prototypical dimensions.

### 8.2.1.3 Scalability of the ORNL/THTF Uncovered-Bundle Heat Transfer Test

The objective of heat transfer testing was to acquire a heat transfer coefficient and fluid conditions in a partially uncovered bundle. The THTF contains a 64-rod electrically heated bundle with internal dimensions typical of a 17x17 PWR fuel assembly. The scaling of the facility is acceptable because it adopts full length and prototypical dimensions.

### 8.2.1.4 Scalability of the ORNL/THTF High-Pressure Reflood Test

The THTF has a 64-rod, full-length rod bundle heat transfer loop. Rod diameter and pitch are typical of a 17x17 PWR fuel assembly. The scaling of the facility is acceptable because it adopts full length and prototypical dimensions.

### 8.2.1.5 Scalability of the UPTF Full-scale SG Plenum CCFL Test

Since UPTF hot leg separate effect test is full scale model, scaling is not an issue.

### 8.2.1.6 Scalability of the Dukler Air-Water Flooding test

Verification of the experimental results was carried out using general correlation using dimensionless parameters in Reference 5.2.1.6-2. Dimensionless groups which relate momentum fluxes are shown as follows:

$$j_g^* = j_g \rho_g^{1/2} [gD(\rho_f - \rho_g)]^{-1/2} \quad (8.2.1.6-1)$$

$$j_f^* = j_f \rho_f^{1/2} [gD(\rho_f - \rho_g)]^{-1/2} \quad (8.2.1.6-2)$$

Correlations for flooding in vertical tubes may be expressed in the general form

$$j_g^{*1/2} + m j_f^{*1/2} = C \quad (8.2.1.6-3)$$

For turbulent flow  $m$  is equal to unity. The value of  $C$  is found to depend on the design of the ends of the tubes and the way in which the liquid and gas are added and extracted. For tubes with sharp-edged flange,  $C = 0.725$ , when end effects are minimized,  $C$  lies between 0.88 and 1.0. Hewitt and Wallis found that for an air-water system the flooding velocities could be correlated by the equation

$$j_g^{*1/2} + j_f^{*1/2} = 0.88 \quad (8.2.1.6-4)$$

## 8.2.2 Integral Effect Tests (IETs)

### 8.2.2.1 ROSA-IV/LSTF small break (5%) LOCA test (SB-CL-18)

The LSTF is an experimental facility designed to model a full height primary system of the reference PWR. The four primary loops of the reference PWR are represented by two equal-volume loops. The overall facility scaling factor is 1/48. The overall scaling factor was used as follows:

- Elevations: preserved, i.e., one to one correspondence with the reference PWR. Because the LSTF hot and cold leg inner diameters (IDs) are smaller than those of the reference PWR, only the elevations of the top of the primary hot and cold legs were set equal to those of the reference PWR.
- Volumes: scaled by the facility scaling factor 1/48.
- Flow area: scaled by 1/48 in the pressure vessel and 1/24 in the steam generators. However, the hot and cold legs were scaled to conserve the ratio of the length to the square root of pipe diameter, i.e.,  $L/\sqrt{D}$  for the reference PWR. Such an approach was taken to better simulate the flow regime transition in the primary loops. In other words, the hot and cold legs were sized to conserve the volume scaling and the ratio of the length to the square root of pipe diameter,

- 
- $L/\sqrt{D}$ , for the reference PWR in expectation that the flow regime transitions in the primary loops can be simulated appropriately by taking this scaling approach.
  - Core power: scaled by 1/48 at core powers equal to or less than 14% of the scaled reference PWR rated power. The LSTF rated and steady-state power is 10 MWt, i.e., 14% of the rated reference PWR core power scaled by 1/48. With this scaled core power, a reduced core inlet flow rate can be obtained and the condition of the steam generator secondary side is changed to accommodate the scaled power.
  - Fuel assembly: dimensions, i.e., fuel rod diameter, pitch and length, guide thimble diameter pitch and length, and ratio of number of fuel rods to number of guide thimbles, designed to be the same as the 17x17 fuel assembly of the reference PWR to preserve the heat transfer characteristics of the core. The total number of rods was scaled by 1/48 and is 1064 for heated and 104 for unheated rods.
  - Design pressures: approximately the same as the reference PWR.
  - Fluid flow differential pressures ( $\Delta P$ s): set to be equal to the reference PWR for scaled flow rates.
  - Flow capacities: scaled by the overall scaling factor where practicable.

---

## **REQUEST 5-1**

### Section 5.2

The prototype plant in the scaling analysis of the test facilities is a reference PWR and not the US-APWR. Though the reference PWR is a 4-loop plant with 17x17 fuel assemblies, there are significant differences between the reference PWR and the US-APWR, e.g. active fuel height (12 ft. for the reference and 14 ft. for the US-APWR) and number of grid spacers (9 for the reference PWR and 11 for the US-APWR). Provide an evaluation of the impact of not using US-APWR design parameters in the scaling analysis.

## **RESPONSE**

In principle, there is no impact of not implementing US-APWR's fuel assembly design parameters such as the active fuel length of 14 ft instead of 12 ft. The top grid spacer #1 and the bottom grid spacer #11 do not contribute to the change of scalability. The intrinsic neutronics and thermal-hydraulics characteristics are maintained in the nine (9) grid spacers to be the same as that of reference plants. The additional 2 ft is to accommodate the additional grid spacers.

The US-APWR fuel design uses 11 grid spacers that span the 14-ft active fuel length. The upper and lower grid spacers are made of nickel-chromium-iron Alloy-718 (Inconel 718), and the nine intermediate grid spacers are made of Zircaloy-4. The influencing parameter is the span between grids. The grid span for the US-APWR design is almost the same as that for the 12-ft Mitsubishi fuel with a 9 grid spacer design. The intermediate grid spacer is designed based on current version in use in Mitsubishi-fueled reactors with advanced mixing vanes. Additionally, the reduced power density in 14-ft fueled PWR compared to that of 12-ft moderates the impact by having an added thermal margin for PCT.

The response to REQUEST 8.1-1 contains the evaluation results of US-APWR design parameters in the scaling analysis. MHI has performed a comparison of the main fuel and core design parameters between the US-APWR and conventional PWR. As shown in Table RAI-8.1-1.2 and Table RAI-8.1-1.3 in the response to REQUEST 8.1-1, it is confirmed that the difference does not cause negative impact or introduce new phenomenon. It is clarified that the effect of differences are properly simulated by the code and can be concluded that the conventional (reference) model is applicable to the US-APWR.

## **REQUEST 6-1**

### Section 6.1.2

The M-RELAP5 documentation must be reasonably self-contained. The existing references for M-RELAP5 in the topical report refer to documentation for RELAP5-3D and RELAP5Mod3.3 extensively. There are no stand-alone M-RELAP5 code manuals. Provide stand-alone M-RELAP5 manuals and in particular a user manual on how to call for the EM models in M-RELAP5.

## **RESPONSE**

A stand alone M-RELAP5 input manual has been developed based on the RELAP5-3D input manual, with the addition of the features of Appendix-K model. The document has been submitted to the US-NRC as follows: "**M-RELAP5 Input Manual, 6AS-1E-UAP-080014(R0), Proprietary**", which is the derivation of RELAP5-3D Volume II, Appendix A: Input Data Requirements. Table RAI-6-1.1 summarize on how to find the Appendix-K EM in the M-RELAP5 input manual.

There are no others stand-alone manuals for M-RELAP5. The rest are the same as for RELAP5-3D Code Manuals, prepared by the RELAP5-3D Code Development Team, Idaho National Laboratory, INEEL-EXT-98-00834, Revision 2.4, published in June 2005, consisting of:

- Volume I: Code Structure, System Models and Solution Methods
- Volume II: User's Guide and Input Requirements
- Volume IV: Models and Correlations
- Volume V: User's Guidelines

The RELAP5-3D is not equipped with a particular Volume III. It uses the previously prepared Volume III manual for RELAP5/Mod3, entitled: RELAP5/Mod3 Code Manual Volume III: Developmental Assessment Problems (Draft), NUREG/CR-5535, EGG-2596 (Draft), INEL, June 1990.

Table RAI-6-1.1 Correspondence of Appendix-K EM to M-RELAP5 input manual

No.	Important Parameters of Appendix-K Requirements	Corresponding Sections and Pages in M-RELAP5 Input Manual
1	Initial Stored Energy (Gap conductance model consistent with the fuel design code is installed)	Cards 1CCCGXNN, Heat Structure Input - Card 1CCCG001, Gap Conductance Model Initial Gap Pressure Data, p8-3
2	Fission Product Decay (ANS standard 1971 is installed)	Section 15 Cards 30000000 through 30099999, 15.3 Card 30000002, Fission Product Decay Information, p15-3.
3	Metal Water Reaction Rate (The Baker-Just equation is installed)	Section 8.3 Card 1CCCG003, Metal-Water Reaction Control: W1(R) Initial oxide thickness on cladding's outer surface (m, ft). Add 1.0 (m ft) to initial oxide thickness to use <b>Baker-Just oxidation model</b> , p8-4.
4	Cladding Swelling and Rupture ✓ Cladding swelling and rupture model for ZIRLO™ alloy is installed. ✓ Gap conductance calculation for rupture node is installed.	Section 8.4 Card 1CCCG004, Fuel Cladding Deformation Model Control. W2(I) ZIRLO model flag. Enter 0 if ZIRLO cladding deformation model is not to be calculated. Enter 1 if ZIRLO cladding deformation model is to be calculated. Either a 0 or a 1 must be entered, p8-4.
5	Discharge Model (The Moody model is installed)	2.1 Card 1, Developmental Model Control. Option 22. This option uses Moody critical flow model rather than modified Henry-Fauske critical flow model. This option has no effect if the modified Henry-Fauske critical flow model is not selected.
6	Return to Nucleate Boiling (The logic to prevent return to nucleate boiling during blowdown is installed)	Section 8.15 Card 1CCCG800, Additional Left Boundary Option. W3(I) Flag for CHF degradation model at high void fraction. Enter 0 if CHF degradation model is not to be calculated. Enter 1 if CHF degradation model is to be calculated. Either a 0 or a 1 must be entered, p8-15
7	Return to Transition Boiling (The logic to prevent return to transition boiling during blowdown is installed)	The same as above.

**REQUEST 6-3**

Section 6.2.1.3

In Table 6.2.1-4a why does the separator component not apply for the secondary side of SG?

**RESPONSE**

Reviewer is correct. It is a typo. The separator component does apply for the secondary side of SG. The Table has been revised accordingly.

## **REQUEST 4-1**

### Section 4.2

Report identifies five phases of the SBLOCA transient. However, boundaries of these phases are not clearly defined. Provide parameters that indicate when one phase ends and other begins.

## **RESPONSE**

In order to identify various phenomena, a small break LOCA transient can be divided into five periods: blowdown, natural circulation, loop seal clearance, boil-off, and core recovery. The duration of each period depends on the break size and the performance of the ECCS. The following discussion of these five periods assumes that the small break occurs in the cold leg, as a limiting location to the peak cladding temperature (PCT). The periods during small break LOCA are described as follows:

### **Blowdown period**

The blowdown period starts from the initiation of the break. It ends when the primary system pressure has decreased to nearly equal the secondary system pressure.

Upon initiation of the break, the primary side of the reactor-coolant system (RCS) rapidly depressurizes until the hot coolant flashes into vapor. Reactor trip is automatically initiated on the low pressurizer pressure setpoint of 1860 psia (for the US-APWR). Then, the reactor coolant pump (RCP) will trip automatically at reactor trip. For the US-APWR LOCA analysis, the RCPs automatically trip, after 3 seconds delay following the reactor trip. The ECCS actuation signal is generated when the pressurizer pressure decreases to the low pressurizer pressure setpoint of 1760 psia (US-APWR) and the high-head safety injection initiates, after a time delay. Loss of condenser steam dump effectively isolates the steam generator (SG) secondary side, causing it to pressurize to the safety valve set point of [ ] psia (US-APWR), and release steam through the safety valves. During this blowdown phase, the break flow is single-phase liquid. The coolant in the RCS also remains in the liquid phase throughout most of the blowdown period, although towards the end of the blowdown period, phase separation (vapor formation) starting to occur in the upper head, upper plenum and hot legs. Finally, the rapid depressurization ends when the RCS reaches a pressure just above the steam generator secondary side pressure. This ends the blowdown period.

### **Natural Circulation period**

The natural-circulation period starts at the end of blowdown. It ends when the liquid flow rate at the top of SG u-tubes decreases to zero.

At the end of the blowdown period, two-phase natural circulation is established when the RCS reaches a quasi-equilibrium condition with duration depending on break size. Another indication is that the RCP head pressure shall be zero to initiate natural circulation. During this period, loop seal formation occurs in the cross-over leg, the piping between the SG outlet and the inlet of RCP. The loop seals remain plugged and the system drains from the top to down with voids beginning to form at the top of the SG tubes and continuing to form in the upper head and top of the upper plenum region. The decay heat is removed by heat transfer (condensation and convection) to the SG secondary side during this time. The emergency feedwater is initiated to maintain the secondary side inventory. Vapor

generated in the core is trapped within the RCS by the loop seal (liquid plug). As more low quality coolant flow exits the break, the vapor accumulates in the downhill side of the SG tubes and the crossover leg. The natural circulation will continue until driving-head on the cold leg side of the loops is no longer sufficient, due to the accumulation of steam in loops between the top of the steam generator tubes and the loop seals. In another word, the mass flowrate at the top of SG tubes shall be zero to indicate the end of natural circulation.

#### **Loop Seal Clearance period**

The loop-seal clearance period starts when natural circulation ends. The period ends when the liquid level on the downhill side of the steam generator reaches the elevation of the loop seal and steam is vented towards the break.

With the loop seals present, the break remains covered with water. The RCS coolant inventory continues to decrease and steam volume in the RCS increases. The relative pressure in the core increases, which, together with the loss of coolant inventory through the break, causes the liquid levels in the core and the SG to continue to decrease. If, during this process, the core mixture-level drops below the top of the core, a core uncover occurs, and the cladding temperature in the upper part of the core will begin to heat up. The core uncover can be a rapid and deep level drop but short in duration. When the liquid level of the downhill side of the SG is depressed to the elevation of the loop seals, the seals clear and steam initially trapped in the RCS can be vented through the break. The break flow changes from initially a low quality mixture to primarily steam. As the pressure imbalances throughout the RCS are restored, the back pressure in the core is relieved. Then, the core liquid level is restored to the cold leg elevation with the coolant flowing from the downcomer.

#### **Boil-off period**

The boil-off period starts after the loop seals clear and ends when the minimum RCS inventory is reached.

After the loop seal clearing, the RCS primary-side pressure continues to fall below that of the secondary-side caused by the continuous coolant outflow from the break with an increasing flow-quality. This process signifies the gradual boil-off of the liquid inventory in the reactor vessel that consequently decreases the mixture-level therein (i.e. in the core). The decreasing rate would be even higher if the RCS pressure is too high for the ECCS to compensate the boil-off rate. In some cases, the decrease in mixture level will reach a minimum value that result in a deep core uncover. The boil-off period ends when the core collapsed liquid level reaches a minimum. At this time, the RCS has depressurized to the accumulator setpoint of 600 psia (for US-APWR). The accumulator will inject ECCS water to the RCS at a rate higher than the break flow.

#### **Core Recovery period**

The core recovery starts at the end of the boil-off period and ends when the fuel rod cladding in the entire core is quenched by a low-quality mixture.

Eventually, the combined flowrates supplied by the high-head safety injection and the accumulator exceed the break flow. The vessel mass inventory increases and the core recovery is established. The accumulator injection into the core begins before the coolant is completely discharged into the containment, and the RCS pressure is still significantly above the containment pressure. The core recovery indicates the end of small break LOCA, when all parts of the core is quenched and covered by a low quality mixture.

## **REQUEST 4-2**

### Section 4.2

Report (Page 4-4) indicated that relative pressure in the core increases. Explain what is relative pressure? How does it decrease liquid level in the core? (Loop Seal Clearance)

## **RESPONSE**

The description of the loop seal clearance period will be clarified as follows:

The loop-seal-clearance period starts when natural circulation ends. The period ends when the liquid level on the downhill side of the steam generator reaches the elevation of the loop seal and steam is vented towards the break.

With the loop seals present, the break remains covered with water. The RCS coolant inventory continues to decrease and steam volume in the RCS increases. During loop seal formation, the hydrostatic pressure difference that develops in the SG tubes depresses the liquid level in the core. This phenomenon is due to the difference in void fraction and mixture densities on the two sides of the SG. The uphill side of the SG is in countercurrent flow, with steam flowing upwards and liquid flowing downwards. The downhill side experiences co-current flow, with both phases flowing downwards. The mixture density is higher in the uphill side compared to the downhill side, which may generate a considerable hydrostatic pressure difference due to the height of the tubes.

This pressure difference is transmitted to the two-phase level in the core through the hot leg. As a result, the core is pressurized relative to the downcomer and a considerable portion of core inventory may be forced out from the core. If, during this process, the core mixture-level drops below the top of the core, a core uncover occurs, and the cladding temperature in the upper part of the core will begin to heat up. The core uncover can be rapid and deep, but is short in duration. When the liquid level on the downhill side of the SG reaches the elevation of the loop seals, the seals clear and steam initially trapped in the hot portions of the RCS can be vented to the break.

The break flow changes from initially a low-quality mixture to primarily steam. As the pressure imbalances throughout the RCS are restored, the back pressure in the core is relieved. Then, the core liquid level is restored to the cold leg elevation with coolant flowing from the downcomer to the core

**REQUEST 4-3**

Section 4.2

What is mechanism of loop seal clearing? It is not clear from the description.

**RESPONSE**

The responses to REQUESTs 4-1 and 4-2 above provide an improved description of the loop seal clearing mechanism. Figures RAI-4-3.1 and RAI-4-3.2 show the mechanisms of loop-seal formation and clearance.

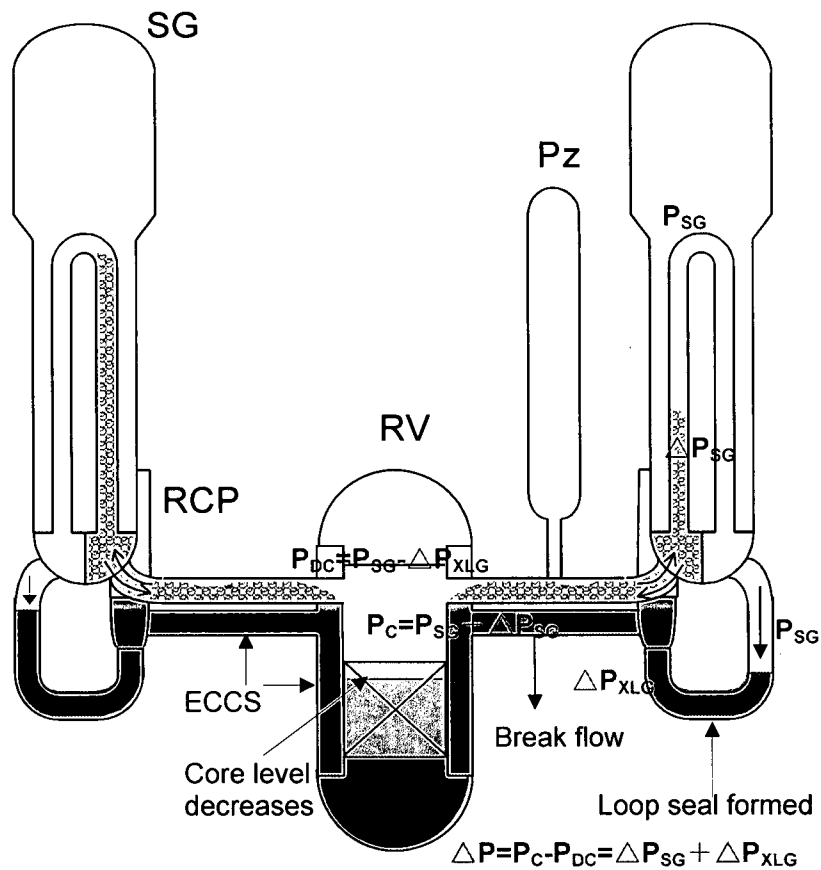


Figure RAI-4-3.1 Mechanism of loop seal formation

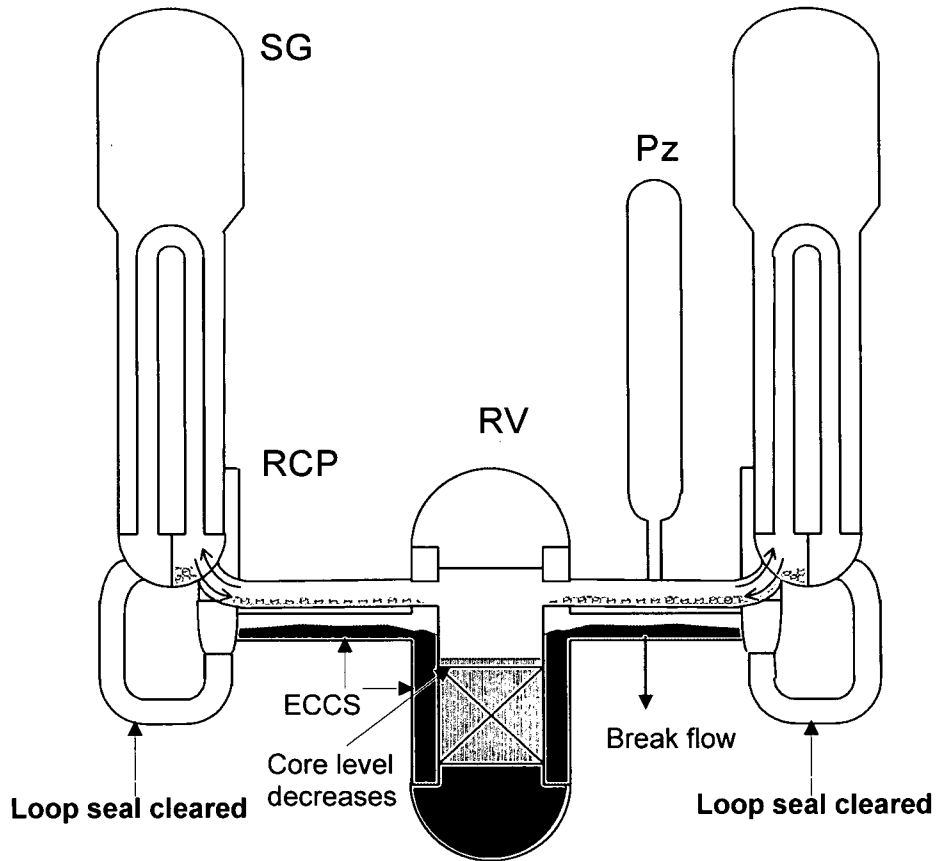


Figure RAI-4-3.2 Mechanism of loop seal clearing

**REQUEST 4-4**

[Empty box for Request 4-4]

**RESPONSE**

[Empty box for Response]

**REQUEST 4-5**

[ ]

**RESPONSE**

[ ]

**REQUEST 4-6**

[Empty response area for Request 4-6]

**RESPONSE**

[Empty response area for Response]

#### **REQUEST 4-7**

##### Section 4.3.2.7

Pressurizer pressure is used as a parameter for reactor trip and safety injection signal. Vapor generation in the primary system will have strong influence on this pressure. Explain why interfacial mass transfer or flashing has not been identified as a phenomenon of interest.

#### **RESPONSE**

The interfacial mass transfer or flashing is identified as a phenomenon of interest in a postulated large-break LOCA, during the blowdown period, where depressurization rate is much higher than that of small-break LOCA. In addition, all phenomena are judged based on their impact to the PCT calculation. Although vapor generation in the primary system, especially in the uncovered core has a strong influence on pressure, its impact to PCT is relatively low. For all PWR systems and US-APWR, the reactor trip and safety injection pressure setpoints of 1860 psia and 1760 psia, respectively, are reached before bulk flashing occurs in the core. Finally, the initiation of flashing in the upper head strongly depends on the initial coolant temperature, not only pressure, and does not occur before the setpoints are reached.

**REQUEST 4-8**

Section 4.3.2.9

The report mentions that for smaller breaks the loop seal may not clear. During Loop Seal Clearing period, what is the status of safety injection (including accumulator flow) for various break sizes? (PIRT-45)

**RESPONSE**

Sensitivity studies were performed and documented in the Technical Report accompanying the DCD. The technical report cites that the loop seal may not clear for break size equal to or smaller than 1-inch.

Stabilization of the primary pressure at a relatively high level during a small-break size prevents injection of the accumulator's borated water for some time, while the boil-off process and break flow will continue to reduce the liquid inventory in the reactor vessel. The accumulator will be initiated once the RCS pressure reduces to 600 psia. Table RAI-4-8.1 provides an insight about the status of ECCS during a small-break LOCA. Once actuated, the HHIS will continue to operate. Accumulator flow was not initiated during the calculations for the smaller breaks shown in the table.

Table RAI-4-8.1 Status of ECCS during a small-break LOCA

No.	Break Size	Loop Seal Status		Status of ECCS throughout Small-Break transient	
		Clear	No Clear	HHIS (SI Pumps) Initiated at (s)	Advanced Accumulator Initiated at (s)
1	2-inch	X		221	Not actuated <sup>1)</sup>
2	3.4-inch (DVI Line)	X		153	Not actuated <sup>1)</sup>
3	7.5-inch	X		130	299
4	1-ft <sup>2</sup>	X		126	90

<sup>1)</sup> Not actuated in the specified duration of this transient calculation

---

## **REQUEST 4-9**

### Section 4.3.2.9

There is some uncertainty as to whether loop seal clearing (PIRT #45) will occur first in the broken loop or in the lumped intact loop (3 loops combined). The effect of loop dynamics (or asymmetric effects) was not included as one of the phenomenon for consideration in the PIRT process. Please explain.

## **RESPONSE**

The reviewer is correct that there are uncertainties on which loop would clear first in a symmetrical 4-loop PWR. However, the proximity to the break favors the broken loop. Also the break size could influence preferential loop seal clearing.

It has been shown by integral effect tests (IETs) performed in the past that normally, the loop-seal in the broken loop will clear first (allow vapor to pass through). When this happens, the stored liquid in the upper parts of the downcomer will fall and the two-phase level in the core will rise rapidly.

MHI believes that the uncertainty in the loop seal clearing process is not caused by the effect of loop dynamics (i.e. asymmetric effects), but due to the uncertainty in the flow regime and its impact on flow resistance through the loop seal. Entrainment and counter-current flow limiting (CCFL) in the uphill of RCP suction leg affects the mass retention in the loop seal piping following the venting. MHI is also in the opinion that as long as the capacity of injection flow rates of SI pumps and accumulator are more than sufficient, the effect of loop asymmetric or unbalanced can be well mitigated.

**REQUEST 4-10**

[ ]

**RESPONSE**

[ ]

**REQUEST 4-11**

Section 4.4

How are medium ranked phenomena treated in the analyses?

Are there any assessments of the medium ranked phenomena?

**RESPONSE**

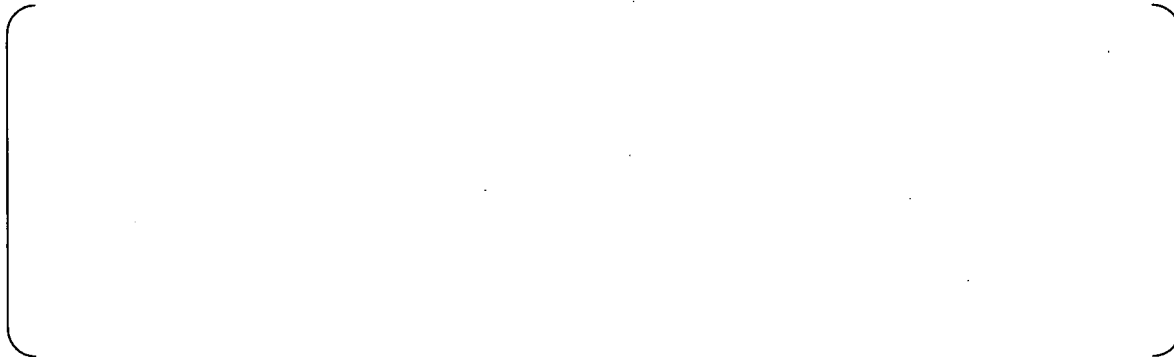


Table RAI-4-11.1 PIRT for Small Break LOCA (Medium-ranked phenomena)

Location Process / Phenomena		Small Break LOCA				
		Blowdown	Natural Circulation	Loop Seal Clearance	Boil-off	Recovery
<b>Fuel Rod</b>						
2	Core kinetics, Reactor Trip (fission power)					
3	Decay Heat					
4	Oxidation of Cladding					
5	Clad Deformation (Creep/Burst)					
<b>Core</b>						
8	Heat Transfer below the Mixture Level					
12	Entrainment/Deentrainment					
13	3-D Flow					
17	Top Nozzle/Tie Plate CCFL					
<b>Neutron Reflector</b>						
<b>Upper Head</b>						
22	Drainage to Core / Initial Fluid Temperature					
23	Bypass Flow between Upper Head and Downcomer (Cold Leg)					
<b>Upper Plenum</b>						
25	Mixture Level					
26	Drainage to Core					
27	Entrainment/Deentrainment					
28	Bypass Flow / Hot Leg - Downcomer Gap					
<b>Hot leg</b>						
30	Stratified Flow/Counter-flow					
31	Entrainment/Deentrainment					
<b>Pressurizer and Surge Line</b>						
<b>Steam Generator</b>						
39	Primary Side Heat Transfer					
40	Secondary Side Heat Transfer (Water Level)					
42	Multi U-Tube Behavior					
43	AFW					
<b>Crossover Leg</b>						
45	Loop Seal Formation and Clearance (Entrainment/Flow Regime/Interfacial Drag/Flow Resistance)					

Asterisk (\*) denotes that the ranking is "break size dependent."

Table RAI-4-11.1(cont'd) PIRT for Small Break LOCA (Medium-ranked phenomena)

Location	Process / Phenomena	Small Break LOCA				
		Blowdown	Natural Circulation	Loop Seal Clearance	Boil-off	Recovery
<b>Reactor Coolant Pump</b>		<div style="border: 1px solid black; border-radius: 15px; width: 100%; height: 100%;"></div>				
48	Coastdown Performance					
<b>Cold Leg</b>						
51	Stratified Flow					
52	Steam Condensation by ACC Water					
<b>Accumulator</b>						
56	Large Flow Injection/ Flow Resistance					
<b>Downcomer/Lower Plenum</b>						
60	Mixture Level/Void Distribution					
62	ECCS Water/Mixing					
64	DVI/SI Water/Flowrate					
65	DVI/SI Water/Condensation					
66	DVI/SI Water/ Injection Temperature					
<b>Break</b>						

Asterisk (\*) denotes that the ranking is "break size dependent."

## **REQUEST 4-12**

### Section 4.4.2

What does confirmation mean?

What are the criteria of confirmation?

## **RESPONSE**

Confirmation in this context means the analyses performed using M-RELAP5 to validate the important models related to high-ranking phenomena. The criterion of confirmation is that if there are phenomena, models and/or parameters that are of important interest for US-APWR SBLOCA scenario or certain test activities, then those items must be verified and validated through comparisons with experimental data or independent calculations. The objectives are (1) to judge whether a model can be categorized as best-estimate or conservative in calculating the PCT, and (2) to verify that for each H-ranked phenomenon, the Appendix-K model is conservative.

Table 4.3.2-2 is the SBLOCA PIRT showing the high-ranking phenomena. The H-ranked phenomena consist of 2 categories. The first category contains those phenomena for which M-RELAP5 is judged to have a best-estimate capability, such as models related to the core mixture level and the countercurrent flow limiting (CCFL) models. In consideration that M-RELAP5 is almost the same with RELAP5-3D, the implementation of the Appendix-K model does not cause any impact to these models. Therefore, we can expect best-estimate results. The second category contains phenomena that are directly affected by the Appendix-K model, such as decay heat and modifications to the heat transfer logic that directly affect the PCT calculation. Applying these models yields conservative results (the PCT is higher than that calculated using the BE approach).

## **REQUEST 7-1**

Table 7.1.1-1(4/4)

Appendix K requirement #15 ECC water bypass is taken as not applicable to SBLOCA. The bypass flow between upper head and downcomer could potentially provide a path for steam to enter the downcomer during the loop seal clearance period. Confirm that none of the SBLOCA analyses, including sensitivity cases, experience the effect of steam impeding ECC flow.

## **RESPONSE**

As a complete core uncover does not occur in SBLOCA transients, the vapor generated in the core does not directly escape into the break through the downcomer. Then, the ECC water bypass phenomenon which is typical for LBLOCA transients will not occur in SBLOCA transients.

As the loops are sealed at the cross-over legs during the loop seal clearance period, upper head/downcomer bypass flow path has the potential for relieving vapor generated in the core. The break size spectrum analyses for the cold leg break are performed for US-APWR (Ref.1). The loop seal clearance periods for various break sizes are shown in Figure RAI-7-1.1. The assumed break orientation for these cases is the bottom of the cold leg. ECC water injection start time of the high head safety injection systems and the accumulators are also shown in Figure RAI-7-1.1. Only the high head safety injection system injects ECC water during the loop seal clearance period.

ECC water from the high head safety injection systems is injected into the downcomer in the downward direction between the vessel wall and the barrel wall through the direct vessel injection line shown in Figure RAI-7-1.2. So, even if the steam flow through the bypass line exists, it does not impede ECC flow into the core.

The collapsed liquid level transients in the vessel upper head and the end of the loop seal clearing period for several break sizes are shown together with top of bypass line elevation in Figure RAI-7-1.3. The bypass line is covered by the water during the loop seal clearance period. So, the vapor generated in the core hardly escape to the downcomer through the bypass line.

For these reasons, ECC flow will not be impeded by the steam flow through the upper head/downcomer bypass line for the cold leg break with the break orientation of bottom.

Following sensitivity analyses are also performed for US-APWR (Ref.1).

- Break Orientation (bottom, top and side of cold leg)
- Break Location (cold leg, hot leg, crossover leg, DVI injection line, pressurizer steam phase)
- Noding near break point
- Noding of SG U-tube and crossover leg
- Time Step Size
- No single Failure Assumption
- Offsite Power Available

As the effect of break orientation on the RCS behavior is negligible small, break orientation hardly affects the loop seal clearance period, the ECC water injection start time, and the collapsed liquid level in the vessel upper head. Then, impeding of ECC water by steam flow does not occur in the calculation with any break orientation.

As the loop seal formation will not occur in the cases of hot leg, crossover leg and pressurizer steam phase break, impeding of ECC water by steam flow will not occur. As

only ECC water from the high head safety injection systems is injected during the loop seal clearance period in the DVI injection line break, impeding of ECC water by steam flow does not occur as in the cold leg break.

None of the sensitivity analyses of the nodding and time step size experience impeding of ECC water by steam flow, as the sensitivities to these parameters are small.

The sensitivity analyses for no single failure assumption and offsite power available are performed for 7.5 inch and 1.0ft<sup>2</sup> cold leg breaks. The loop seal formation occurs only in 7.5 inch break. ECC water injection will not occur during loop seal clearance period for the case of no single failure assumption, and only ECC water from the high head safety injection systems is injected during the loop seal clearance period for the case of offsite power available. Then, impeding of ECC water by steam flow will not occur in both cases.

#### References

1. MHI, Small Break LOCA Sensitivity Analyses for US-APWR, MUAP-07025-P (R0), December 2007.

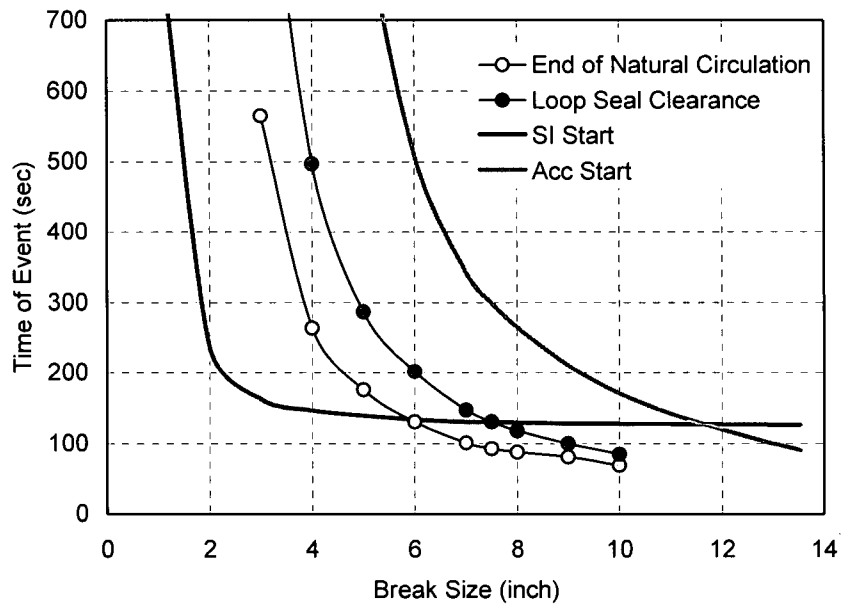


Figure RAI-7-1.1 Loop seal clearance period and SI/Acc injection start time

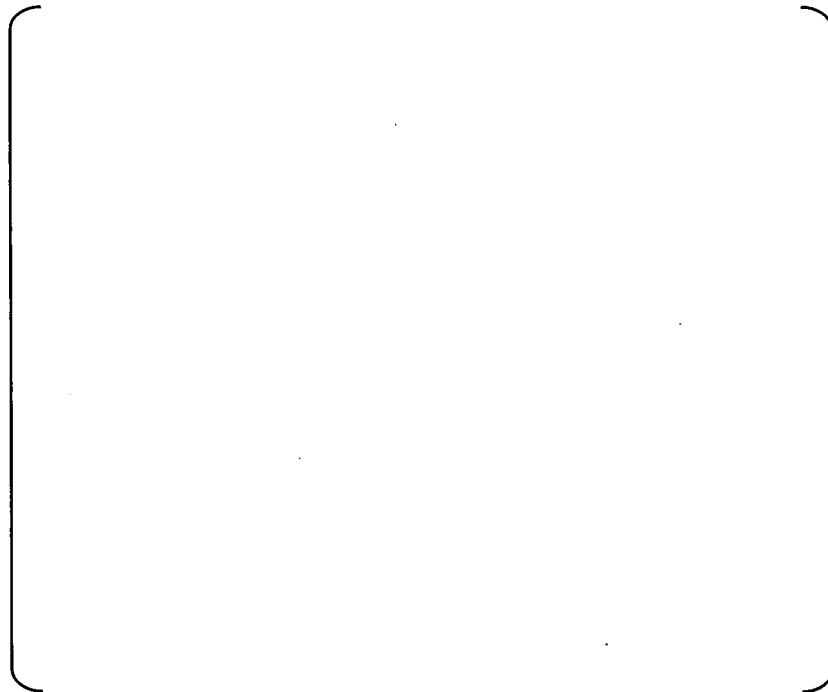


Figure RAI-7-1.2 ECC water flow from the high head safety injection systems

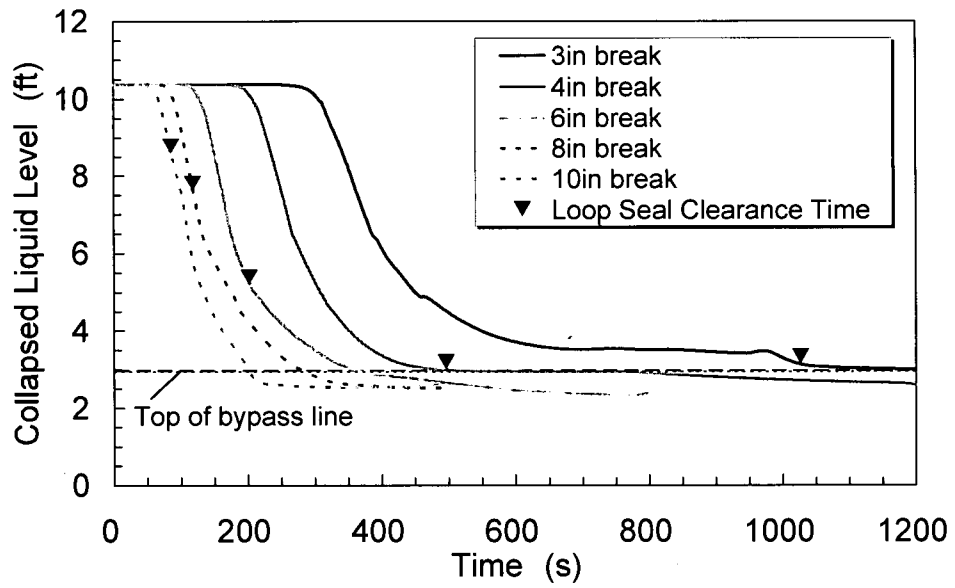


Figure RAI-7-1.3 Collapsed liquid level in the vessel upper head

## **REQUEST 7-2**

Table 7.1.1-1(4/4)

Appendix K requirement #29 refill/reflood heat transfer is taken as not applicable to SBLOCA. However, there could be core uncover during the loop seal clearance period resulting in cladding superheat. Confirm that all SBLOCA cases do not require refill/reflood heat transfer. If they do require refill/reflood heat transfer then explain why Appendix K requirement #29 is not for SBLOCA.

## **RESPONSE**

Appendix K requirement #29 requires that an applicable FLECHT heat transfer correlation shall be used for reflood rates of one inch per second or higher. And it also requires that when reflood rates are less than one inch per second, heat transfer calculations shall be based on the assumption that cooling is only by steam rather than a FLECHT heat transfer correlation, and shall take into account any flow blockage due to cladding swelling or rupture. The requirement #29 limits the use of a FLECHT heat transfer correlation. As a FLECHT heat transfer correlation is not used in M-RELAP5, this requirement is taken as not applicable to SBLOCA. But, additional form loss coefficients due to flow blockage are applied in M-RELAP5 when a fuel rod ruptures in accordance with the requirement #29.

The reflood heat transfer after the core uncovers is calculated by the heat transfer package incorporated in M-RELAP5, and it is validated by ORNL/THTF high-pressure reflood tests.

**REQUEST 7-3**

Section 7.1.2

The discussion of gap conductance model is in the form of one equation and one reference to the fuel design code FINE. Provide validation analysis of the gap conductance model as expressed in Equation (7.1.2-1). Provide verification of the implementation of the gap conductance model in M-RELAP5 and demonstrate the integration of the gap conductance model with the rest of the gap heat transfer model in RELAP5-3D, such as thermal radiation across the gap.

**RESPONSE**

The following gap conductance model considering pellet offset in the fuel-cladding gap is incorporated in RELAP5-3D (Ref.1).

$$h_g = \frac{k_g}{N} \sum_{n=1}^N \frac{1}{t_n + 3.2(R_F + R_C) + (g_1 + g_2)} \quad (1)$$

Where

- $h_g$  = conductance through the gas in the fuel-cladding gap
- $n$  = number of circumferential segment
- $N$  = total number of circumferential segments = 8
- $k_g$  = thermal conductivity of gas
- $t_n$  = width of fuel-cladding gap at the n-th circumferential segment
- $R_F, R_C$  = surface roughness of the fuel and cladding
- $g_1, g_2$  = temperature jump distance terms for fuel and cladding

Fuel temperature calculated by FINE is used in SBLOCA analysis as an initial fuel temperature. The gap conductance model incorporated in FINE is given by

$$\left( \begin{array}{l} \text{---} \\ \text{---} \\ \text{---} \end{array} \right) \quad \begin{array}{l} (2) \\ (3) \\ (4) \end{array}$$

Where

- $h_{gap}$  = conductance through the gas in the fuel-cladding gap (Btu/hr-ft<sup>2</sup>-deg F)
- $k_{mix}$  = gas mixture thermal conductivity (Btu/hr-ft-deg F)
- $gap$  = diametral gap (in)
- $EXO$  = surface roughness factor

The gap conductance model incorporated in FINE is validated in combination with other models through assessment calculations that compare the code prediction results to fuel temperature measurement data. The results of validation study are reported in the topical report of Mitsubishi Fuel Design Criteria and methodology (Ref.2).

Equation (3) for smaller gap is applied to calculate the fuel temperature for SBLOCA. As the consistent gap conductance model with equation (3) in FINE is required in SBLOCA analysis, the original gap conductance model in RELAP5-3D is transformed into the following concentric gap conductance model.

$$h_g = \frac{k_g}{g + 3.2(R_F + R_C) + (g_1 + g_2)} \quad (5)$$

Where

$g$  = concentric fuel-cladding gap width

As the temperature jump distance terms in equation (5) are considered in the gas mixture thermal conductivity in equation (3), both equations are equivalent.

The gap conductance is calculated by M-RELAP5 and FINE at equivalent conditions and is compared to verify that the gap conductance model is adequately implemented in M-RELAP5.

Analytical conditions are followings.

Cladding outer diameter: 0.374 in

Cladding thickness: 0.0224 in

Pellet diameter: 0.322 in

Pellet density: 97 %TD

Burn up: 0.0 MWD/T

Radial power distribution in pellet: flat distribution is assumed.

[ Core pressure: 2250 psia ]

M-RELAP5 nodding scheme is shown in Figure RAI-7-3.1. Heat structure HS010 represents a fuel rod, and single volume SV010 represents fluid volume containing the fuel rod. Vapor temperature of time dependent volume TV100 is selected so that the calculated cladding surface temperature agrees with that predicted by FINE. Pressure of time dependent volume TV400 is adjusted to make the SV010 pressure to be 2250psia. Internal pressure calculated by FINE is used in M-RELAP5. The input values for surface roughness of the fuel and cladding for M-RELAP5 are selected so that the effect of surface roughness on gap conductance is same between M-RELAP5 and FINE.

The comparisons of the calculated gap conductance by M-RELAP5 and FINE are shown in Figure RAI-7-3.2. The gap conductance is also calculated by M-RELAP5 using the pellet offset gap conductance model presented in equation (1). The pellet offset gap conductance model gives larger values than FINE. On the other hand, gap conductance with the concentric gap conductance model agrees with the prediction by FINE. However, a small difference remains between the two predictions. Two causes are pointed out. First, the gap conductance by M-RELAP5 includes the additional thermal radiation term across the gap. But, its contribution to the gap conductance is too small at normal conditions to explain the difference as discussed later. Next, as M-RELAP5 uses the same thermal expansion models for cladding and fuel as RELAP5-3D, the applied thermal expansion models for cladding and fuel are different between M-RELAP5 and FINE. These differences affect the predicted gap size by each code. The gap conductance calculated by M-RELAP5 is divided by the ratio of gap size calculated by FINE to gap size calculated by M-RELAP5. The obtained gap conductance agrees well with that by FINE shown in Figure RAI-7-3.3. It is concluded that the concentric gap conductance model consistent with FINE is adequately implemented in M-RELAP5.

In addition to the conductance through the gas in the fuel-cladding gap, the following thermal radiation across the fuel-cladding gap is considered in RELAP5-3D.

$$h_r = \sigma F (T_F^2 + T_C^2) (T_F + T_C)$$

$$F = \frac{1}{\left\{ \frac{1}{\varepsilon_F} + \left( \frac{R_F}{R_C} \right) \left[ \frac{1}{\varepsilon_C} - 1 \right] \right\}} \quad (6)$$

Where

- $h_r$  = conductance by thermal radiation across the gap
- $\sigma$  = Stefan-Boltzmann constant
- $F$  = view factor
- $\varepsilon_F, \varepsilon_C$  = emissivity of fuel and cladding
- $R_F, R_C$  = outer radius of fuel and inner radius of cladding
- $T_F, T_C$  = temperature of fuel outer surface and temperature of cladding inner surface

M-RELAP5 uses the same thermal radiation term as RELPA5-3D. Radiation gap conductance mainly depends on the gap average temperature, and slightly depends on the ratio of outer fuel radius to inner cladding radius. Radiation gap conductance dependency on the average gap temperature is shown in Figure RAI-7-3.4.

As the gap average temperature is less than 1000 deg F under the normal operating conditions, the radiation gap conductance is less than 10 Btu/ft<sup>2</sup>-h-F. It is less than 1% compared with the gap conductance through the gas in the gap, and it can be neglected under the normal operating conditions. However, radiation gap conductance increases as the gap average temperature rises, and the gap conductance through the gas in the gap decreases when the cladding swelling or rupture occurs under LOCA transient. The contribution of radiation gap conductance can not be neglected under LOCA. So, the radiation gap conduction term is implemented in M-RELAP5. Radiation gap conductance is calculated at a SBLOCA simulated condition by M-RELAP5. Calculations are performed using nodding scheme shown in Figure RAI-7-3.1 and the same conditions as the previous study except the followings.

- Linear power density: 0.0617kW/ft (power at decay heat level)
- Core pressure: 1000 psia

Fuel rod temperatures are increased by setting the vapor temperature of time dependent volume TV100. The obtained radiation conductance is shown in Figure RAI-7-3.4. It agrees with the prediction with equation (6). It is concluded that the radiation conductance model across the gap is adequately implemented in M-RELAP5.

#### References

1. RELAP5-3D CODE MANUAL VOLUME I: CODE STRUCTURE, SYSTEM MODELS, AND SOLUTION METHODS, INEEL-EXT-98-00834, Revision 2.4, June 2005.
2. MHI, Mitsubishi Fuel Design Criteria and Methodology, MUAP-07008-P, May 2007.

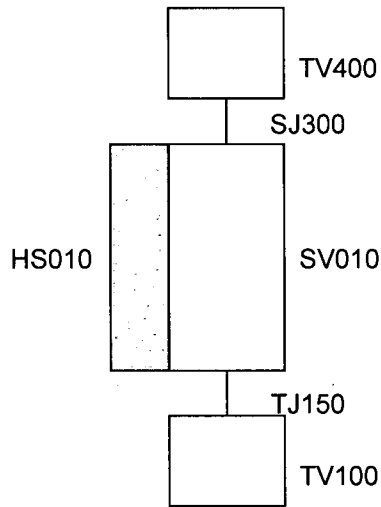


Figure RAI-7-3.1 M-RELAP5 noding scheme

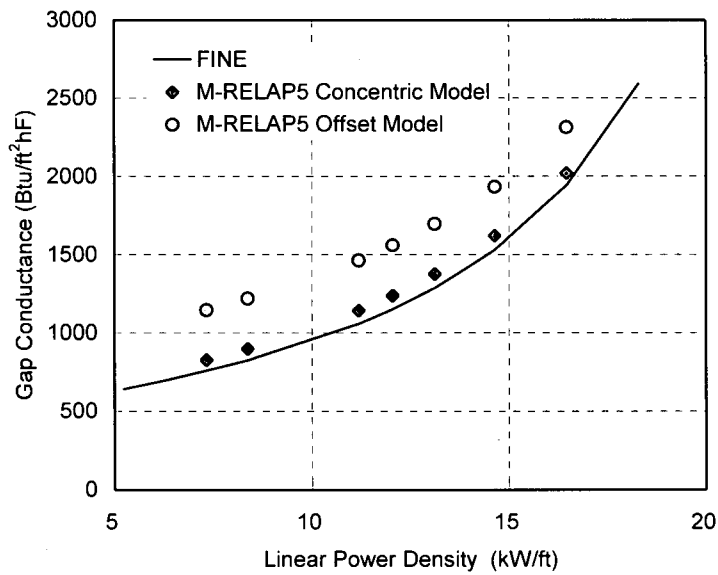


Figure RAI-7-3.2 Comparisons of the gap conductance

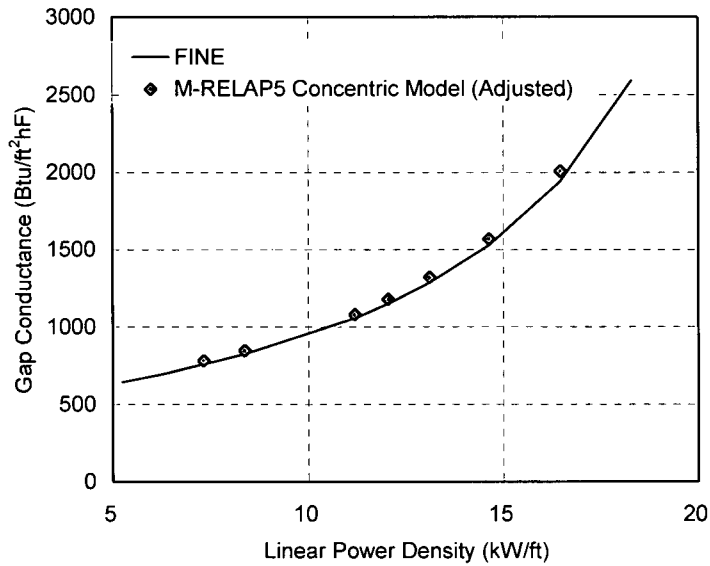


Figure RAI-7-3.3 Comparisons of the gap conductance (gap size is adjusted)

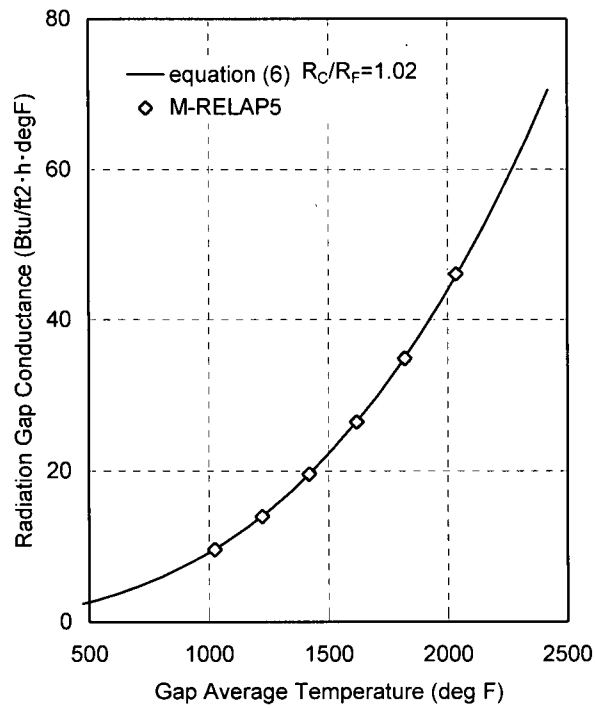


Figure RAI-7-3.4 Radiation gap conductance dependency on gap average temperature

**REQUEST 7-4**

Section 7.1.3

Provide a reference or fuel cycle calculation to justify the claim that the default values of the ANSI/ANS 5.1-1979 standard are appropriate for the US-APWR and yield the highest decay heat from the actinide series.

**RESPONSE**

The default values described in the topical report include the yield of  $^{239}\text{U}$  produced per a nuclear fission, the released energy from the decay of an actinide nucleus and the decay constant. The released energy from the decay of an actinide nucleus and the decay constant are particular values for each actinide nucleus. These values, therefore, are independent from fuel cycle calculation of the US-APWR and are appropriate for the US-APWR.

On the other hand, the yield of  $^{239}\text{U}$  produced per a nuclear fission is dependent on the fuel specifications, especially, the fuel enrichment and the fuel burnup. Figure RAI-7-4.1 shows that the calculation results of the US-APWR based on its expected fuel enrichment were covered by the default value 1.0 in M-RELAP5 over the broad fuel burnup. Therefore, it is conservative to use the default value 1.0.

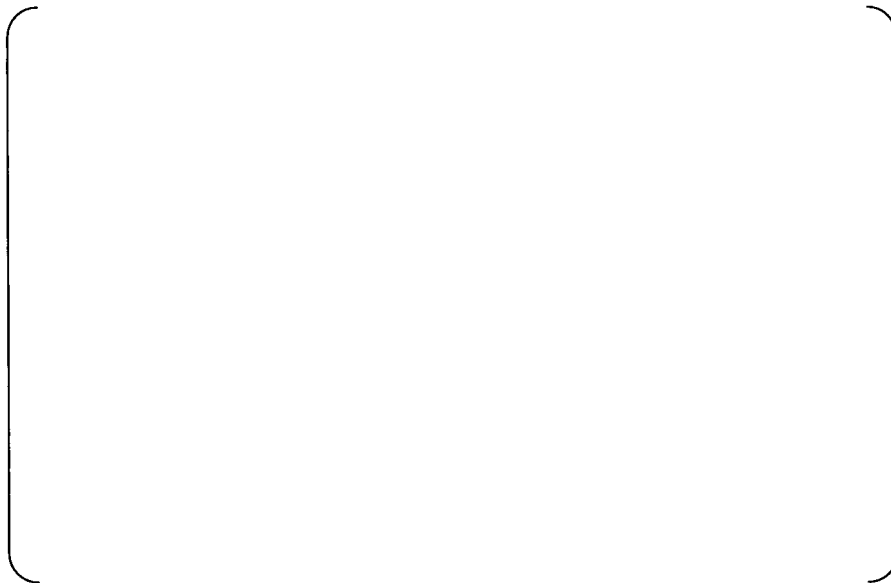


Figure RAI-7-4.1 Yield of  $^{239}\text{U}$  produced per a nuclear fission

**REQUEST 7-5**

Section 7.1.4.1

Provide verification of the implementation of the Metal Water Reaction Rate Model in M-RELAP5. Confirm that the hydrogen generation rate and the heat generation rate are consistent with the metal/water reaction rate.

**RESPONSE**

The thickness of the cladding converted to oxide, the metal-water reaction heat release rate, and hydrogen mass generated by the metal-water reaction at an isothermal condition are calculated by M-RELAP5 and are compared with analytical calculation results to verify that the Baker-Just correlation is adequately implemented in M-RELAP5.

The assumed analytical conditions follow.

Fuel rod specification: 17x17 fuel rod (cladding outer diameter is 9.5mm)

Initial oxide thickness: 0.0mm

Oxidation temperature: 1200 deg C constant

Oxidation time: 100sec

M-RELAP5 nodding scheme is shown in Figure RAI-7-5.1. Heat structure HS010 represents a fuel rod with 100mm axial length, and single volume SV010 represents fluid volume containing the fuel rod. Vapor temperature of time dependent volume TV100 is set to be 1200 deg C and junction vapor flow of time dependent junction TJ150 is set to be  $1.0 \times 10^6$  kg/s to maintain the cladding surface temperature at 1200 deg C. Fluid pressure is maintained to be 10MPa by time dependent volume TV400. Fission and decay heat power are neglected and a large rod surface heat transfer coefficient is applied so that the metal-water reaction heat rate can be estimated from the heat transfer rate from cladding to vapor. Cladding swelling and rupture calculations are skipped so that the M-RELAP5 and analytical results can be easily compared.

The Baker-Just correlation is given by

$$W^2 = 33.3 \times 10^6 t \exp\left[-\frac{45,500}{RT}\right] \tag{1}$$

Where

- $W$  = the amount of zirconium reacted (mg/cm<sup>2</sup>)
- $t$  = the time (s)
- $R$  = the gas constant, 1.987 (cal/mole-K)
- $T$  = the temperature (K)

The amount of zirconium reacted can be expressed in terms of the thickness of the cladding reacted for convenience as follows.

$$W = 100 \times \rho_{Zr} \delta = 6.5 \times 10^5 \delta \tag{2}$$

Where

- $\rho_{Zr}$  = zirconium density, 6500 (kg/m<sup>3</sup>)
- $\delta$  = the thickness of cladding reacted (m)

Substituting equation (2) into equation (1) gives:

$$\delta = \sqrt{33.3 \times 10^6 t \exp\left[-\frac{45,500}{RT}\right]} / 100 \rho_{Zr} = \sqrt{33.3 \times 10^6 t \exp\left[-\frac{45,500}{RT}\right]} / 6.5 \times 10^5 \tag{3}$$

Equation (3) gives the thickness of cladding reacted at constant temperature.

The amount of reacted zirconium weight per unit length is given by

$$M = \rho_{Zr} \pi \{r_0^2 - (r_0 - \delta)^2\} = \rho_{Zr} \pi \{2r_0 \delta - \delta^2\} \quad (4)$$

Where

$$\begin{aligned} M &= \text{the amount of reacted zirconium weight per unit length (kg/m)} \\ r_0 &= \text{the cladding outer radius (m)} \end{aligned}$$

Differencing equation (4) for the time gives the reacted zirconium weight per unit length and per unit time as follows.

$$\begin{aligned} \frac{dM}{dt} &= 2\rho_{Zr} \pi (r_0 - \delta) \frac{d\delta}{dt} = \rho_{Zr} \pi (r_0 - \delta) \sqrt{33.3 \times 10^6 \exp\left[\frac{-45,500}{RT}\right]} \frac{t^{-0.5}}{100\rho_{Zr}} \\ &= \pi (r_0 - \delta) \sqrt{33.3 \times 10^6 \exp\left[\frac{-45,500}{RT}\right]} \frac{t^{-0.5}}{100} \end{aligned} \quad (5)$$

As reaction heat release incorporated in M-RELAP5 is  $5.94 \times 10^8$  J/(kg · mol), and molecular weight of zirconium is 91.22 kg/(kg · mol), the reaction heat release rate per unit length is given by

$$Q'_{MWR} = \pi (r_0 - \delta) \sqrt{33.3 \times 10^6 \exp\left[\frac{-45,500}{RT}\right]} \frac{t^{-0.5}}{100} \times \frac{5.94 \times 10^8}{91.22} \quad (6)$$

Where

$$Q'_{MWR} = \text{the reaction heat release rate per unit length (W/m)}$$

The total hydrogen mass generated by the metal-water reaction is calculated by multiplying the mass of zirconium reacted by the ratio of the four hydrogen atoms to one zirconium atom. Then, the total hydrogen mass generated by the metal-water reaction per unit length is given by

$$M_{H2} = M \times \frac{4.0}{91.22} = \rho_{Zr} \pi \{2r_0 \delta - \delta^2\} \times \frac{4.0}{91.22} \quad (7)$$

Where

$$M_{H2} = \text{the total hydrogen mass generated by metal-water reaction (kg/m)}$$

The comparisons of the calculated results of the zirconium reacted thickness, the reaction heat release rate and the hydrogen mass generated by M-RELAP5 with the results by equation (3), equation(6) and equation (7) are shown in Table RAI-7-5.1 and Figure RAI-7-5.2, Figure RAI-7-5.3 and Figure RAI-7-5.4. The calculated results by M-RELAP5 agree with the results by the analytical method well. It is concluded that the Baker-Just correlation is adequately implemented in M-RELAP5 and the hydrogen generation rate and the heat generation rate are also adequately calculated.

Table RAI-7-5.1 Comparison between analytical method and M-RELAP5

time (sec)	Reacted Zirconium Thickness(m)		Reaction Heat (W/m)		H2 Generation (kg/m)	
	Equation(3)	M-RELAP5	Equation(6)	M-RELAP5	Equation(7)	M-RELAP5
5	8.36426E-06	8.36433E-06	1054.7	1054.7	7.10889E-05	7.10894E-05
10	1.18289E-05	1.18288E-05	745.27	745.26	1.00498E-04	1.00498E-04
20	1.67285E-05	1.67283E-05	526.44	526.44	1.42052E-04	1.42051E-04
30	2.04882E-05	2.04879E-05	429.49	429.49	1.73909E-04	1.73906E-04
40	2.36577E-05	2.36573E-05	371.70	371.70	2.00746E-04	2.00742E-04
50	2.64501E-05	2.64496E-05	332.27	332.26	2.24374E-04	2.24370E-04
60	2.89747E-05	2.89741E-05	303.15	303.15	2.45724E-04	2.45720E-04
70	3.12962E-05	3.12956E-05	280.53	280.52	2.65348E-04	2.65342E-04
80	3.34571E-05	3.34564E-05	262.29	262.28	2.83604E-04	2.83598E-04
90	3.54866E-05	3.54858E-05	247.18	247.18	3.00743E-04	3.00736E-04
100	3.74061E-05	3.74053E-05	234.40	234.40	3.16946E-04	3.16940E-04

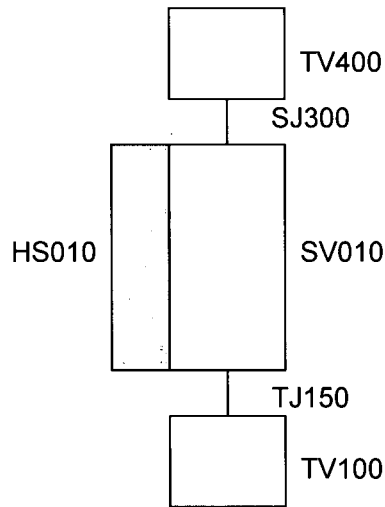


Figure RAI-7-5.1 M-RELAP5 noding scheme

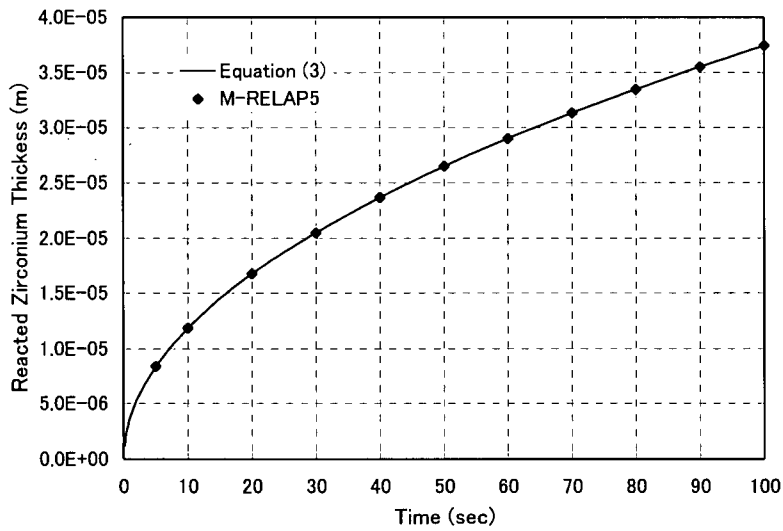


Figure RAI-7-5.2 Comparison of the thickness of zircaloy reacted

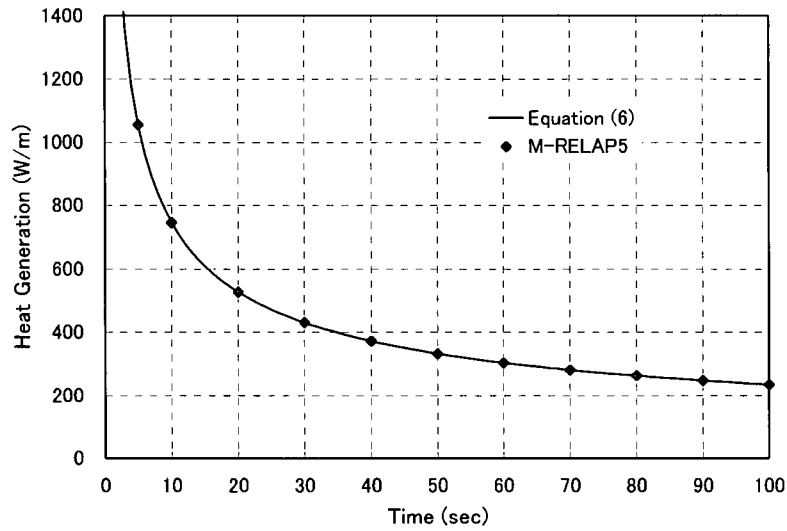


Figure RAI-7-5.3 Comparison of the reaction heat release rate

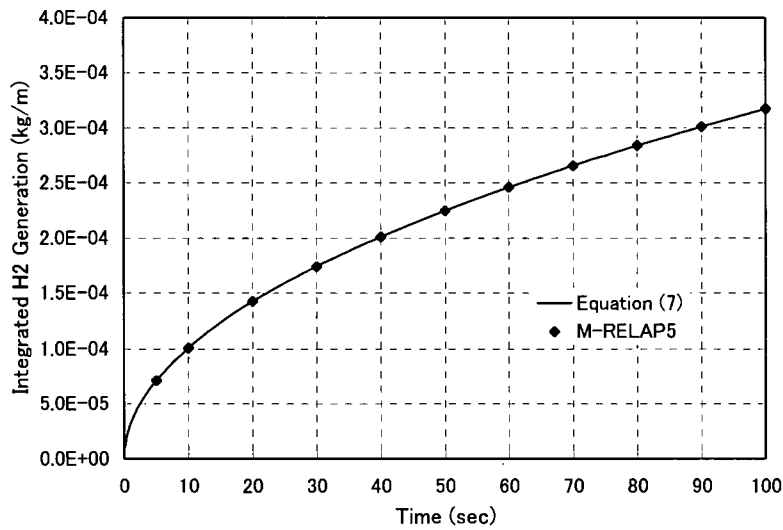


Figure RAI-7-5.4 Comparison of the hydrogen mass generated

**REQUEST 7-6**

Section 7.1.4.2

Verify the correctness of the exponential term in Equation (7.1.4-8). It appears a negative sign is missing.

**RESPONSE**

The Equation (7.1.4-8) in the topical report is shown here again. There is certainly a negative sign in the exponent term.

$$dr_n = \left[ (d\tilde{r}_{n-1})^2 + K\Delta t e^{-\frac{A}{RT}} \right]^{1/2} \quad (7.1.4-8)$$

**REQUEST 7-8**

[Empty response box for Request 7-8]

**RESPONSE**

[Empty response box]



**REQUEST 7-9**

Section 7.1.6

It appears with non-condensable quality, the two-phase critical flow will be calculated by using the extended Henry-Fauske model instead of the Moody model. Explain this switch in two-phase critical flow model. The operation of the advanced accumulator may introduce non-condensable to the system. Did the SBLOCA analysis ever reach a state that required the use of the extended Henry-Fauske model?

**RESPONSE**

The pressure of the advanced accumulator when nitrogen gas begins to flow out is around [ ] psia. In the analysis of core-cooling performance during the course of small-break LOCA's periods, the primary system pressure is considerably higher than the nitrogen flow-out pressure, even for the maximum break size case, as shown in Figure RAI-7-9.1. Therefore, small-break-LOCA analysis for the US-APWR does not result in any state that requires the use of the extended Henry-Fauske model.

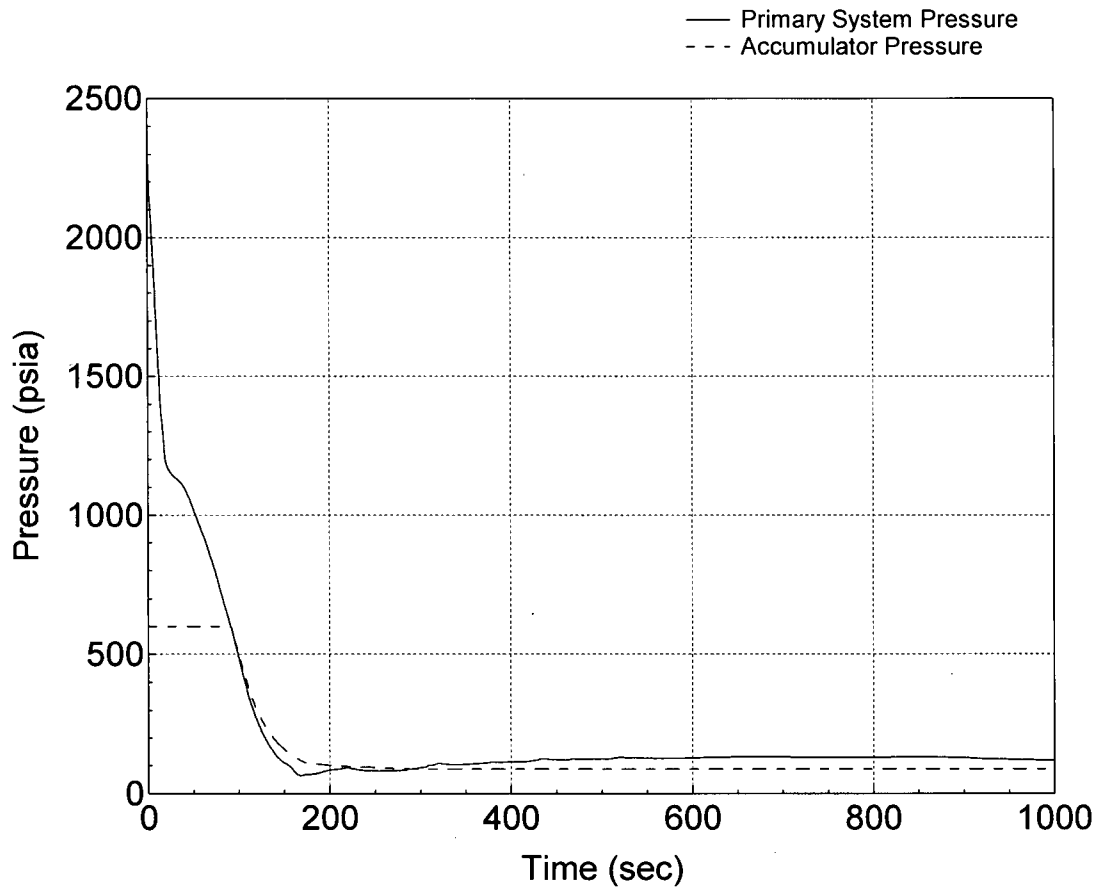


Figure RAI-7-9.1 Primary System and Accumulator Pressure for 1ft<sup>2</sup> Cold-Leg Break

**REQUEST 7-12**

Section 7.1.7.6

The logic to prevent return to nuclear boiling and transition boiling is only necessary (per Appendix K) during the blowdown phase of a LOCA. Provide the criteria used to define the blowdown phase when the prevention logic is applicable.

**RESPONSE**

SBLOCA transients are generally divided into five periods: blowdown, natural circulation, loop seal clearance, boil-off and core recovery. The boundaries of these periods are described in the response to REQUEST 4-1. The blowdown period starts from the initiation of the break. It ends when the primary system pressure has decreased to nearly equal the secondary system pressure. The blowdown period is generally followed by the natural circulation and loop seal clearance periods during SBLOCA transients.

Even if CHF or excess cladding over-heating occurs in the early stage of the blowdown period, the return to nucleate boiling or the return to transition boiling can be expected soon after the reactor trip because the rod surface heat flux greatly reduces and the sufficient coolant exist in the core. However, these rewetting phenomena are not validated by any experimental data. Therefore, the prevention logic of the Appendix K requirement is conservatively applied during over the blowdown period in the SBLOCA analysis.

Return to nucleate boiling after CHF or return to transition boiling after excess cladding over-heating during loop seal clearance or core recovery periods due to the core mixture level recovery is validated by ORNL/THTF high pressure reflood tests and the ROSA-IV/LSTF test. Therefore, the prevention logic is not necessary for these periods.



## **REQUEST D-2**

Appendix D also describes uncertainty in Cv. A set of questions were asked in Topical report on Adv Accumulator (MUAP-07001) and LBLOCA Methodology report (MUAP-07011), and will not be repeated here.

## **RESPONSE**

MHI understands that NRC does not expect a specific response from MHI to this particular REQUEST, as a set of questions were raised in the Topical Reports for Advanced Accumulator and will be raised in the Topical Report for LBLOCA Methodology. MHI response to NRC's questions for the uncertainty in the flow rate coefficients is already presented in UAP-HF-07086-P(R0) (Ref.1). And, when additional questions are raised in the Topical Report for LBLOCA Methodology, MHI will response to them.

### References

1. Response to NRC's Questions for Topical Report MUAP-07001-P(R1) The ADVANCED ACCUMLATOR, UAP-HF-07086-P(R0), Mitsubishi Heavy Industries, Ltd., July 2007.

**REQUEST C-1**

[ ]

**RESPONSE**

[ ]

**REQUEST C-2**

Appendix C

What is the impact of the discontinuity exhibited by the right end points of the curves in Figure C-4?

**RESPONSE**

As described in the response to REQUEST 7-8, the under-relaxation method relaxes the magnitude or level of the discontinuity of the critical flow rate. Therefore, no impact is anticipated in the small-break-LOCA analyses for the US-APWR.

### **REQUEST 8-1**

#### Section 8.0

M-RELAP5 was created by modifying RELAP5-3D. Does any of the change have a direct impact on the result of the M-RELAP5 assessment? Are the differences in the results produced by using M-RELAP5 and RELAP5-3D consistent with the differences in the two codes?

### **RESPONSE**

M-RELAP5 has been developed and assessed for its application to the SBLOCA analysis for US-APWR without altering the original features of its base code, RELAP5-3D.

The primary feature of the M-RELAP5 evaluation model is that the code is applicable to the SBLOCA analysis and satisfies the conservative requirements prescribed in 10 CFR 50, Appendix K, "ECCS Evaluation Models." In developing M-RELAP5, several conservative models and correlations have been implemented in its base code, RELAP5-3D. M-RELAP5 has also incorporated the model of the advanced accumulator, which is the only new engineered safety feature specific to US-APWR when compared to other 4-loop PWR plants.

Unless the models specific to M-RELAP5 are switched on, M-RELAP5 is identical to RELAP5-3D in terms of its calculation results.

## **REQUEST 8-2**

Section 8.0

Was a single frozen version of M-RELAP5 used in all the assessments presented in this section? If yes, was the same version of M-RELAP5 used in the SBLOCA analysis?

## **RESPONSE**

A single frozen version of M-RELAP5 was used in all the assessments presented in Section 8.0 of the topical report. A slightly different yet ultimately the same version of M-RELAP5 was used in the SBLOCA analysis for the preparation of the Design Control Document (DCD) for the US-APWR (Ref.1).

The difference between the two M-RELAP5 versions used in the calculations for the topical report and the DCD consists only in the difference in the way to read in the input data, i.e., the READ format. There is no difference between the two versions to make the calculation results of the two versions different.

Therefore it can be concluded that the two versions of M-RELAP5 used in the SBLOCA analyses for the topical report and the DCD are ultimately the same.

### References

1. MHI, Design Control Document for US-APWR, Chapter 15 Transient and Accident Analyses, MUAP-DC015 Revision 0, December 2007.

### **REQUEST 8.1-1**

Discuss the scaling of each test in Sections 8.1.1 (ROSA-IV LSTF) and 8.1.2 (ORNL/THTF) vs. US-APWR (in terms of vessel and rod heights, volume, flow areas, rod diameter, power/heat flux ratio, grid spacers, ratio of heated and unheated rods, and SG elevation, tube diameter and tube length, etc.), and justify the scaling (i.e., why the differences in these scales, if any, are not an issue) in using these tests for the US-APWR assessment.

### **RESPONSE**

To validate M-RELAP5, the Phenomena Identification and Ranking Table (PIRT) for small break LOCA in the US-APWR has been developed. The phenomena ranked as "High" in the PIRT have been either conservatively modeled based on the Appendix-K requirements or confirmed by validation of the corresponding models in M-RELAP5 through simulations of selected tests. Table RAI-8.1-1.1, which is Table 4.4.2-1 in the Topical Report MUAP-07013-P(R0), lists the simulated tests for the validation of M-RELAP5 along with the high-ranking phenomena for which models have been validated for small break LOCA analysis for US-APWR.

Referring to Table RAI-8.1-1.1, the ROSA-IV/LSTF separate effect test was conducted for the assessment of the core mixture level, which is strongly dependent on the void fraction profile. The core mixture level was also assessed through the ORNL/THTF separate effect test programs. The ORNL/THTF separate effect test facility was also used in the uncovered core heat transfer and reflood tests to investigate the phenomena of CHF / core dryout, uncovered core heat transfer, and rewetting.

Since the ROSA-IV/LSTF and ORNL/THTF tests mentioned in this REQUEST were separate effect tests considering only the core thermal-hydraulic phenomena as described above, the scaling of the core parameters for ROSA-IV/LSTF and ORNL/THTF are described and discussed against a typical 4-loop PWR and the US-APWR in Tables RAI-8.1-1.2 and RAI-8.1-1.3, respectively. Overall, both ROSA-IV/LSTF and ORNL/THTF are quite well scaled with respect to US-APWR.

The key parameters in CHF/rewetting phenomena are the hydraulic diameter and heated diameter. These parameters in the THTF test facility were adequately scaled as shown in Table RAI-8.1-1.3. In addition, the grid span is another important parameter, because the droplet impingement on the grid spacers causes significant effect on the CHF/rewetting behaviors. However, the CHF/rewetting phenomena assessed by the THTF test data are limited only to the reflood condition, where the flooding velocity is relatively low and few droplets are generated. Therefore, the grid span can be excluded from the key parameters. It is noted that significant generation of droplet might occur in a LOCA transient having larger break size, because both the HHIS and ACC flow are injected to the sufficiently depressurized primary system. Consequently, this results in the higher flooding flow rate. Under such a condition, the grid effect tends to facilitate the rewetting behavior. However, the current M-RELAP5 has no model that specifically accounts for this phenomenon, which is conservative from the viewpoint of code application to SBLOCA analyses.

As for the uncovered core heat transfer, the vapor Reynolds number can be the most important parameter, because it dominates the convective heat transfer from the wall to

vapor. No design parameter would affect the vapor Reynolds number, while the test conditions such as thermal power and flow rate can be carefully discussed for the code assessment.

The key parameter in the core mixture level is the void profile. The void profile is primarily sensitive to the flow geometry and hydraulic diameter except the test conditions (pressure, flow rate, thermal power and so on). The flow geometry employed in both the LSTF and THTF tests was the rod bundle which adequately simulated the 17X17 PWR fuel assembly. Thus, their hydraulic diameters were adequately scaled against US-APWR as shown in Tables RAI-8.1-1.2 and RAI-8.1-1.3.

The heated length is also important parameter for the CHF/rewetting and void profile (mixture level). The LSTF and THTF test facilities were targeting on the existing PWR core with 12-ft active fuel length, while the US-APWR employs the design of 14-ft active fuel length. However, the power density of the US-APWR core is sufficiently comparable with the existing PWR (without power uprate). Therefore, there is basically no significant difference in the thermal-hydraulic behavior between the US-APWR and the reference or existing PWR.

To this end, MHI concludes that the scalabilities of ROSA-IV/LSTF and ORNL/THTF separate effect test facilities are applicable to the US-APWR assessment.

Table RAI-8.1-1.1 Validation Tests for High Ranking Phenomena for Small Break LOCA

	CHF/Core Dryout	Uncovered Core Heat Transfer	Rewet	Core Mixture Level	Water Hold-Up in SG Inlet Plenum	Water Hold-Up in U-Tube Uphill Side	SG Primary and Secondary Heat Transfer	Water Level in SG Outlet Piping	Loop Seal Formation and Clearance	Downcomer Mixture Level/Void Distribution
Separate Effect Tests (SETs)										
ROSA/LSTF Void Profile Test				X						
ORNL/THTF Void Profile Test				X						
ORNL/THTF Uncovered Heat Transfer Test	X	X								
ORNL/THTF Reflood Test		X	X							
UPTF SG Plenum CCFL Test					X					
Dukler Air-Water Flooding Test						X				
Integral Effect Tests (IETs)										
ROSA-IV/LSTF Small Break (5%) LOCA Test	X	X	X	X	X	X	X	X	X	X

Table RAI-8.1-1.2 Scaling of Core Parameters for ROSA-IV/LSTF against PWR and US-APWR

Table RAI-8.1-1.3 Scaling of Core Parameters for ORNL/HTF against PWR and US-APWR

---

**REQUEST 8.1-2**

For each of the tests discussed in Sections 8.1.1, 8.1.2 and 8.1.3 scale the testing power in comparison with the timing of the US-APWR decay power (120% of ANS curve).

**RESPONSE**

The times of the Peak Cladding Temperature (PCT) occurrences after the reactor shutdown (SD) for the US-APWR SBLOCA scenarios were obtained from the US-APWR DCD as shown in Table RAI-8.1-2.1.

The Linear Heat Generation Rates (LHGRs) for the ROSA-IV/LSTF tests selected for the M-RELAP5 assessment are specified in Table RAI-8.1-2.2. The LHGR ranged from 0.92 to 1.28 kW/m.

Figure RAI-8.1-2.1 represents the LHGRs corresponding to the ANS-1971 standard decay heat model and 1.2 times the ANS-1971 standard, which was used in the M-RELAP5 analyses of the US-APWR SBLOCA scenarios, along with the LHGRs for the ROSA-IV/LSTF tests selected for the M-RELAP5 assessment. As shown in Figure RAI-8.1-2.1, the range of the LHGRs for the simulated ROSA-IV/LSTF tests fully covers the range of the LHGRs for the 120% of the ANS-1971 standard decay heat curve at the times of the PCT occurrences after the reactor shutdown for the US-APWR SBLOCA scenarios.

The LHGRs for the ORNL/THTF tests selected for the M-RELAP5 assessment are specified in Table RAI-8.1-2.3. The LHGR ranged from 0.32 to 1.29 kW/m.

Figure RAI-8.1-2.2 represents the LHGRs corresponding to the ANS-1971 standard decay heat model and 1.2 times the ANS-1971 standard, which was used in the M-RELAP5 analyses of the US-APWR SBLOCA scenarios, along with the LHGRs for the ORNL/THTF tests selected for the M-RELAP5 assessment. As shown in Figure RAI-8.1-2.2, the range of the LHGRs for the simulated ORNL/THTF tests fully covers the range of the LHGRs for the 120% of the ANS-1971 standard decay heat curve at the times of the PCT occurrences after the reactor shutdown for the US-APWR SBLOCA scenarios.

Table RAI-8.1-2.1 PCT Time after Reactor Shutdown from US-APWR DCD/SBLOCA

Scenario	CR-In Time <sup>(2)</sup> (sec)	SD Time <sup>(3)</sup> (sec)	PCT Time <sup>(4)</sup> (sec)	PCT-SD Time <sup>(5)</sup> (sec)
CLB 7.5 in	11.1	[ ]	136	[ ]
CLB 1.0 ft <sup>2</sup>	8.7	[ ]	166	[ ]
CR-In Time Duration <sup>(1)</sup> (sec)	[ ]			

- (1) Time duration for the control rod insertion
- (2) Initiating time for the control rod insertion
- (3) Time of the reactor shutdown completed: (3) = (1)+(2)
- (4) Time of the PCT occurrence
- (5) Time of the PCT occurrence after the reactor shutdown: (5) = (4)-(3)
- (2) through (4): Time after the blowdown initiation

Table RAI-8.1-2.2 LHGRs for ROSA-IV/LSTF Tests Simulated by M-RELAP5

Test ID	LHGR (kW/m)
ST-NC-01	0.92
ST-NC-06E	1.01
SB-CL-16L	1.28
Min.	0.92
Max.	1.28

Table RAI-8.1-2.3 LHGRs for ORNL/THTF Tests Simulated by M-RELAP5

Test ID	LHGR (kW/m)	Note
3.09.10J	1.07	Level Swell
3.09.10K	0.32	Level Swell
3.09.10M	1.02	Level Swell
3.09.10N	0.47	Level Swell
3.09.10AA	1.27	Void
3.09.10BB	0.64	Void
3.09.10CC	0.33	Void
3.09.10DD	1.29	Void
3.09.10EE	0.64	Void
3.09.10FF	0.32	Void
3.09.10P	0.997	Reflood
3.09.10Q	1.02	Reflood
Min.	0.32	
Max.	1.29	



Figure RAI-8.1-2.1 Comparison of LHGRs for ROSA-IV/LSTF Tests Simulated by M-RELAP5 and Those for US-APWR SBLOCA Decay Power



Figure RAI-8.1-2.2 Comparison of LHGRs for ORNL/THTF Tests Simulated by M-RELAP5 and Those for US-APWR SBLOCA Decay Power

### **REQUEST 8.1-3**

Sections 8.1.1, 8.1.2 and 8.1.3

The submittal concluded that M-RELAP5 was conservative based on the results of test simulations which used only one nodalization for each test. However, sometimes results can vary depending on nodalization. Discuss if any nodalization sensitivity studies were performed to make sure the results were conservative regardless of the nodalization for each test simulation.

### **RESPONSE**

The M-RELAP5 nodalization schemes for the ROSA-IV/LSTF and ORNL/THTF test simulations were developed to be consistent with the scheme used to model the US-APWR. These schemes have been shown to accurately model important thermal-hydraulic parameters such as liquid levels.

The M-RELAP5 input model for the US-APWR SBLOCA analysis was developed following the INL's RELAP5-3D user's guidelines (Ref.1) for the analyses of Westinghouse-designed PWRs. [

]

The axial nodalization schemes used in the M-RELAP5 simulations of both the ROSA-IV/LSTF and ORNL/THTF test bundles were similar to that used in the US-APWR SBLOCA analyses. The average axial node lengths for both test simulations were about [ ] which is almost the same as that used in the US-APWR SBLOCA analyses.

Since the M-RELAP5 nodalization schemes for the ROSA-IV/LSTF and ORNL/THTF test simulations were developed on the basis of the same noding philosophy as the nodalization scheme used in the US-APWR SBLOCA analyses, no nodalization sensitivity study was performed for each test simulation.

#### References

1. RELAP5-3D<sup>®</sup> Code Manual Volume V: User's Guidelines, INEEL-EXT-98-00834, Revision 2.4, June 2005.

**REQUEST 8.1.1-1**

ROSA is an integral test facility including pressurizer and steam generators (SGs). But the simulations were performed only for the vessel. Are the selected tests vessel only tests, or is the vessel isolated for the simulations?

**RESPONSE**

The vessel was not isolated in the present experiment. However, only the vessel was simulated because this test was conducted under the steady-state condition and MHI judged that the vessel thermal-hydraulics including the core void profile has no significant affect from the rest of the system.

The boundary conditions for the vessel model were obtained from experimental measurements. Specifically, the measured crossover leg flow rate and cold leg temperature were used as boundary conditions at the vessel inlet, and the hot leg pressure was uses as a boundary condition at the vessel outlet.

**REQUEST 8.1.1-3**

[ ]

**RESPONSE**

[ ]

**REQUEST 8.1.1-4**

[ ]

**RESPONSE**

[ ]

**REQUEST 8.1.1-5**

Compare how the grid spacers are modeled in the test and in plant simulations (e.g., flow areas, friction factors), and discuss the impact of these modeling differences, if any, on the void fraction distributions.

**RESPONSE**



References

1. The RELAP5-3D© Code Development Team, 2005, "RELAP5-3D© Code Manual Volume II: User's Guide and Input Requirements," INEEL-EXT-98-00834 Revision 2.4

**REQUEST 8.1.2-1**

Figure 8.1.2-2 shows a "shroud plenum annulus". Is this space filled with water? Is there any water flowing through this space? How is this space handled in the test and the simulation?

**RESPONSE**

As described in Section 5.2.1.2 (a) of MUAP-07013-P (R0), the bottom of the "shroud plenum annulus" was connected to the pressurizer surge line and the top of the annulus to the test section (heater section) outlet. Flow through the annulus was controlled by opening or closing valves equipped in these inlet and outlet lines.

Referring to descriptions in terms of the test procedure (Ref.1), both inlet and outlet line valves were left open to facilitate rapid equalization of the test section and annulus mixture-levels during the boiloff process prior to the measurement. Once steady-state was reached, the lines were closed, thus isolating the annulus from the rest of the system, starting the data scan (about 20 seconds). This operation prohibited unfavorable flow leakage from the test section to the annulus during the data measurement. Hence, mixture level was formulated in the annulus region without any flow communication to the rest of the system during the measurement period.



**References**

1. T. M. Anklam et al., Experimental Investigations of Uncovered-Bundle Heat Transfer and Two-Phase Mixture-Level Swell under High-Pressure Low-Heat Conditions, NUREG/CR-2456, ORNL-5848, 1982.

**REQUEST 8.1.2-2**

[Empty response box for Request 8.1.2-2]

**RESPONSE**

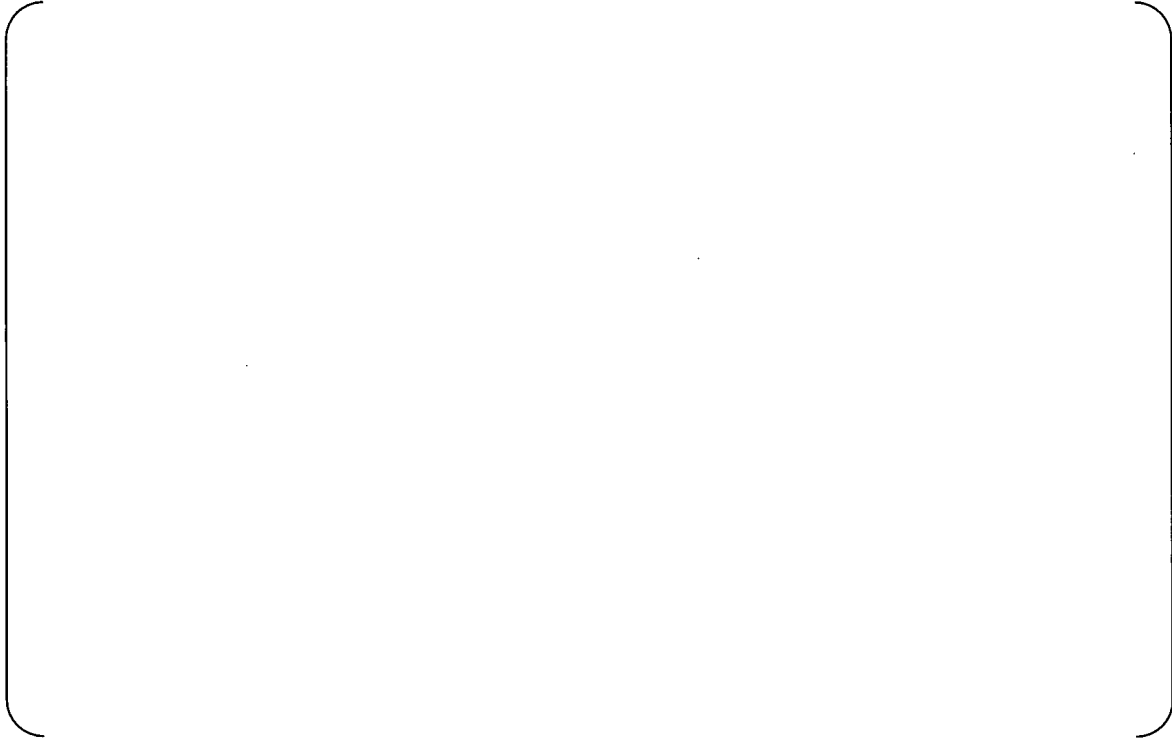
[Empty response box for Response]

**REQUEST 8.1.2-3**

[ ]

**RESPONSE**

[ ]



---

**REQUEST 8.1.2-4**

How is the "measured mixture level" (in Figures 8.1.2-7 and 8.1.2-30) determined in the tests? How is the predicted mixture level (in Figure 8.1.2-30) defined and calculated?

**RESPONSE**

In the experiment, the two-phase mixture level was identified by observing the average temperature at the FRS (fuel rod simulator) thermocouple levels. The measured two-phase mixture levels in Figures 8.1.2-7 and 8.1.2-30 of MUAP-07013-P (R0) were assumed to be midway between the highest level where the average temperature of thermocouples indicated nucleate boiling and the lowest where the average temperature indicated dryout. This is described in Section 5.2.1.2 (4) b of MUAP-07012-P (R0).

Similarly, the two-phase mixture-level predicted by M-RELAP5 was defined to be midway between the highest calculation node where the convective heat transfer mode of the FRS indicated nucleate boiling and the lowest calculation node where the heat transfer mode showed dryout. [

]

### **REQUEST 8.1.2-5**

Section 8.1.2.3 states that "Eventually, the THTF settled into a quasi-steady state with the bundle partially uncovered and inlet flow just sufficient to make up for the liquid being vaporized." Then, please explain why the mass fluxes of Tests K and CC in Table 8.1.2-1 are widely different (2.22 vs. 7.22) for the similar pressure, inlet subcooling and linear heat power. (Comparison of J and AA also.) (Also test FF, which has a higher pressure and higher subcooling, has a higher mass flux, i.e. higher vapor production, than test K for the same power, which is an anomaly). Did all tests result in vaporizing 100% of the incoming liquid? Please provide a table showing the SS energy balance for each test (i.e., Outlet enthalpy- Inlet enthalpy= Heat Input - loss).

### **RESPONSE**

THTF 3.09.10I to N test series was primarily conducted to obtain the heat transfer data in the uncovered-bundle region, where the remarkable two-phase mixture level was formulated in the test section by reducing inlet flow sufficient to make up for the liquid being vaporized. Therefore, much of input thermal power was consumed for steam heat-up to maintain the long uncovered-bundle region.

On the other hand, THTF 3.09.10AA to FF test series was conducted to measure the longer void distribution, where the mixture-level approached the top of the test section as shown in Figures 8.1.2-23 to 8.1.2-28 of MUAP-07013-P (R0). In this latter test series, much of the input power was consumed for coolant boiling, less than the thermal power necessary to maintain longer uncovered-bundle region.

The difference in the generated uncovered-bundle length between two test series induced the different input thermal power (different steady-state heat balance) even under the similar inlet flow, temperature, and pressure conditions, as recognized in comparison between Tests K and CC.

The above explanation is valid also in comparison among Tests K, CC and FF. Test FF had a higher pressure and higher subcooling than Tests K and CC. Hence, Test FF needed higher thermal power to vaporize all the inlet coolant than that of test CC, if inlet flows in Tests CC and FF had been same. Namely, smaller inlet flow was necessary to be fully vaporized in Test FF than Test CC under the same thermal power condition. Finally, Test K resulted in the smaller inlet flow than Tests CC and FF to maintain longer uncovered-bundle region as described above.

Table RAI-8.1.2-5.1 shows the steady-state heat balance based on the measured data for each test (Ref.1). This table validates that input energy meets the exit energy with good accuracy, although slightly large deviations are found in a few cases.

#### References

1. T. M. Anklam et al., Experimental Investigations of Uncovered-Bundle Heat Transfer and Two-Phase Mixture-Level Swell under High-Pressure Low-Heat-Flux Conditions, NUREG/CR-2456, ORNL-5848, 1982.

Table RAI-8.1.2-5.1 Measured Heat Balance Data for THTF 3.09.10 Test Series

Test	(a)FRS Thermal Power (kW)	(b) Heat Loss (kW)	[fraction]	Pressure (MPa)	Mass Flux (kg/m <sup>2</sup> s)	Inlet Temperature (K)	Outlet Temperature (K)	(c) Inlet Flow Energy (kW)	(d) Outlet Flow Energy (kW)	((a)-(b) + (c)-(d))/(d)
3.09.10I	487.19	8.61	[0.018]	4.50	29.76	473.0	774.1	156.24	629.70	0.81%
3.09.10J	234.82	12.13	[0.052]	4.20	12.93	480.3	728.4	70.49	266.53	10.00%
3.09.10K	70.23	12.33	[0.176]	4.01	3.13	466.5	935.0	15.87	73.41	0.48%
3.09.10L	476.22	8.13	[0.017]	7.52	29.11	461.3	715.6	143.76	582.54	5.03%
3.09.10M	223.85	9.46	[0.042]	6.96	13.38	474.4	746.5	70.85	274.69	3.84%
3.09.10N	103.14	16.73	[0.162]	7.08	4.60	473.1	947.9	24.21	108.10	2.33%
3.09.10AA	278.71	5.58	[0.020]	4.04	21.15	450.9	547.0	98.27	373.50	-0.56%
3.09.10BB	140.45	4.83	[0.034]	3.86	9.44	458.2	540.8	45.73	166.98	8.61%
3.09.10CC	72.42	2.53	[0.035]	3.59	7.22	467.6	531.6	36.81	126.91	-15.92%
3.09.10DD	283.10	8.46	[0.030]	8.09	19.82	453.4	595.4	93.67	350.88	4.97%
3.09.10EE	140.45	5.52	[0.039]	7.71	11.00	455.9	581.0	52.71	192.47	-2.51%
3.09.10FF	70.23	6.46	[0.092]	7.53	4.83	451.4	565.8	22.56	83.45	3.46%

**REQUEST 8.1.2-6**

How was the fractional heat loss in Table 8.1.2-1 determined (measured, or calculated to match the energy balance)? Why are they widely different from less than 2% to 17%?

**RESPONSE**

As described in the end of Section 5.2.1.2 (1) b of MUAP-07013-P (R0), heat loss was calculated by ORNL based on the measured thermocouple data. A typical instrumentation site consisted of a pair of thermocouples embedded in the shroud box wall as illustrated in Figure 5.2.1.2-6 of MUAP-07013-P (R0). Because the thermocouples were equipped separately in the radial direction, heat loss could be determined by the temperature gradient. Pairs of thermocouples were settled at the various axial levels as shown in Figure 5.2.1.2-7 of MUAP-07013-P (R0), and each local heat loss was spatially integrated to obtain the total heat loss from the test section.

The test report (Ref.1) describes that the fractional heat loss was dependent on the spatial position, if there existed a longer uncovered-bundle region. Heat loss in the upper portion of the test section was greater than in the lower portion, because the larger temperature gradient across the shroud box occurred in the upper portion due to superheated steam. This indicates that the fractional heat loss was significantly sensitive to the uncovered-bundle length, as demonstrated by the relation between the measured mixture-level and fractional heat loss in Figure RAI-8.1.2-6.1. A relevant description is given in Section 8.1.2.5 of MUAP-07013-P (R0).

References

1. T. M. Anklam et al., Experimental Investigations of Uncovered-Bundle Heat Transfer and Two-Phase Mixture-Level Swell under High-Pressure Low-Heat Conditions, NUREG/CR-2456, ORNL-5848, 1982.

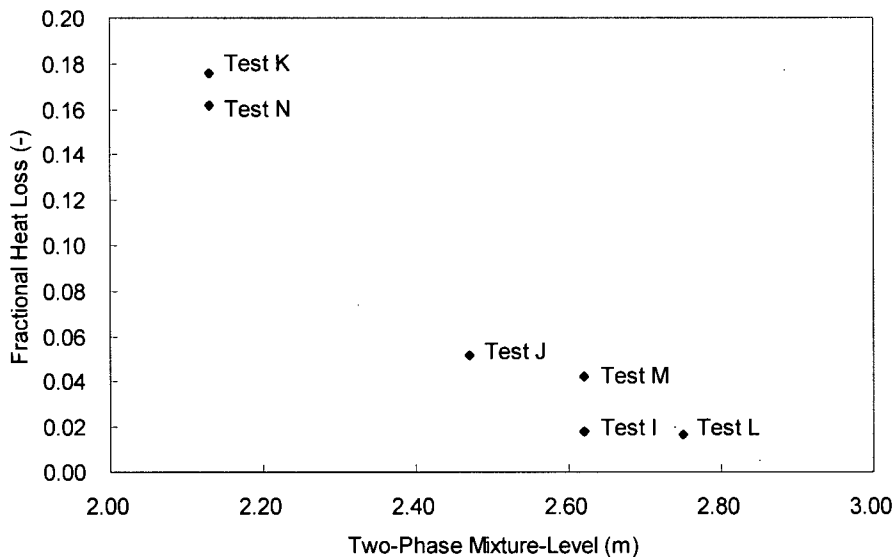


Figure RAI-8.1.2-6.1 Relation between Measured Mixture-Level and Fractional Heat Loss

### **REQUEST 8.1.2-7**

It is observed in Section 8.1.2.5 that "in most cases the calculated void fractions are slightly larger than the experimental values." Please discuss the implication of this observation, particularly in relation to the mixture level. Is this systematic deviation, an indication of the code deficiency?

### **RESPONSE**

M-RELAP5, as well as RELAP5-3D, determines the void profile based on the liquid-vapor interfacial shear derived by the Chexal-Lellouche drift-flux model for the rod bundle geometry. By investigating the calculated results in terms of THTF 3.09.10AA to FF, it is found that M-RELAP5 slightly overestimates the void fraction under the lower pressure condition (Tests AA to CC) and accurately reproduces the measurement under the higher pressure condition (Tests DD to FF). The similar tendency can be recognized in the original report of the Chexal-Lellouche drift-flux model (Ref.1). A tendency observed in the uncovered-bundle heat transfer tests (Tests I to N) is to be discussed in the response to REQUEST 8.1.2-9.

Overestimation in predicted void fraction generally tends to induce the higher two-phase mixture swell. However, its impact is quite limited, because the mixture-level is significantly sensitive to the transition void fraction that defines the boundary from the churn flow regime (two-phase flow) to the mist flow regime (mixture-level generation). The transition void fraction is known to be dependent on pressure, coolant flow and void fraction itself, and affects the velocity slip between liquid and vapor (the liquid-vapor interfacial shear in the two-fluid model as employed in M-RELAP5 code), determining where the mixture-level can be formed. Again, the interfacial shear is determined by the Chexal-Lellouche drift-flux model in M-RELAP5.

In conclusion, M-RELAP5 is able to accurately predict the measured mixture-level as shown in Figure 8.1.2-30 of MUAP-07013-P (R0), which is an evidence that the interfacial shear model in M-RELAP5 is sufficiently valid not only for the void profile prediction but also for the transition void fraction to determine the mixture-level.

#### References

1. B. Chexal and G. Lellouche, A Full-Range Drift-Flux Correlation for Vertical Flows, EPRI-NP-3989-SR Revision 1, 1986.

---

**REQUEST 8.1.2-11**

Provide more detailed explanations of sensitivity study 1. Are these simulations only or also tests? (It appears the measured levels of tests are unchanged. What is the significance of comparing cases of different power level?)

**RESPONSE**

As described in Section 6 and 7 of MUAP-07013-P (R0), M-RELAP5 has been developed based on the best-estimate code RELAP5-3D with inclusion of Appendix K conservative models listed in Table 7.1.1-1. However, no conservative treatment and modification is directly taken into account for the models relevant to the two-phase mixture-level evaluation, thus the M-RELAP5 shows its best-estimate predictability for the mixture-level as shown in Figure 8.1.2-30.

A conservative basis for safety analysis exists in treatment of the thermal power; core decay power is simulated by the ANS 1971 model with multiplication factor of 1.2. This hypothetically causes larger vaporization, inducing longer uncovered-bundle region and slower quench rate. In order to identify this conservatism, MHI had conducted a sensitivity analysis using the THTF mixture-level test data, where the FRS power level was tentatively increased to the 1.2 times of the experimental value for the sensitivity study only. The results are shown in Figures 8.1.2-31 and 32 of MUAP-07013-P (R0) as 'sensitivity 1'. It is found that the predicted mixture-level was conservatively depressed by about 20% in 'sensitivity 1' than the nominal result.

**REQUEST 8.1.2-12**

[ ]

**RESPONSE**

[ ]

**REQUEST 8.1.3-1**

Scale the inlet mass flux in Table 8.1.3-1 in terms of the US-APWR scaling and compare them with the appropriate/typical core inlet flow rate during the reflood period of US-APWR SBLOCA.

**RESPONSE**

Table RAI-8.1.3-1.1 shows a comparison of the experimental flooding mass flux with that expected under the typical SBLOCAs in US-APWR. The US-APWR flooding mass flux data are extracted from the calculations for the core recovery period of the 7.5-in and 1-ft<sup>2</sup> cold leg break accidents described in the design control document (Ref.1). The 7.5-in break generates the highest peak cladding temperature (PCT) during the 'loop seal' period. The 1-ft<sup>2</sup> cold leg break is the limiting case and generates the severest PCT during the 'boiloff' period.

The experimental flooding mass flux conditions are representative of those expected during the typical SBLOCAs in the US-APWR, as shown in Table RAI-8.1.3-1.1.

It is noted that the THTF mass flux data in Table RAI-8.1.3-1.1 are different from the values specified in Table 8.1.3-1 of MUAP-07-13-P (R0), which correspond to the mass flux at the initial steady-state just before the start of the transient. Refer to the response to REQUEST 8.1.3-3.

References

1. MHI, Design Control Document for US-APWR, Chapter 15 Transient and Accident Analyses, MUAP-DC015 Revision 0, December 2007.

Table RAI-8.1.3-1.1 Comparison of Experimental Flooding Velocity with Typical US-APWR SBLOCAs

		Mass Flux	
		(lbm/ft <sup>2</sup> )	(kg/m <sup>2</sup> )
US-APWR	7.5in cold leg break	[ ]	
	1ft <sup>2</sup> cold leg break		
THTF	3.09.10P	16.55	80.80
	3.09.10Q	10.74	52.45

**REQUEST 8.1.3-2**

The flow in Table 8.1.3-1 is given in inlet mass flux (kg/s.m<sup>2</sup>), while the flow in Figure 8.1.3-2 is given in m<sup>3</sup>/s. Revise either so that the units are consistent.

**RESPONSE**

Table 8.1.3-1 of MUAP-07013-P (R0) is to be replaced by the following table so that it keeps consistency with Figures 8.1.3-2 and 5. Additional information is discussed in the MHI response to REQUEST 8.1.3-3.

Table RAI-8.1.3-2.1 Revised ORNL/THTF High-Pressure Reflood Test Conditions

Test	Pressure (MPa)	Initial mass flux (kg/m <sup>2</sup> s)	Initial inlet temperature (K)	Initial inlet subcooling (K)	Linear heat power (kW/m)	Flooding velocity during transient test	
						(cm/s)	(m <sup>3</sup> /s) × 10 <sup>-4</sup>
3.09.10O	3.88	25.36	447.7	74	2.03	12.2	7.50
3.09.10P	4.28	12.19	462.6	65	0.997	9.2	5.66
3.09.10Q	3.95	12.68	456.8	66	1.02	5.9	3.63
3.09.10R	7.34	27.64	449.2	113	2.16	11.7	7.20
3.09.10S	7.53	13.82	459.0	105	1.38	10.2	6.27

---

**REQUEST 8.1.3-3**

The inlet mass flux in Table 8.1.3-1 is not consistent with the flooding velocity of Table 5.2.1.4-4, or Figures 8.1.3-2 and -5. (e.g., Table 8.1.3-1 show similar inlet mass flux for Tests P and Q, but Figure 8.1.3-2 for Test P and Figure 8.1.3-5 for Test Q show substantially different flow rates). Clarify the discrepancy (the same applies to tests R and S).

**RESPONSE**

The inlet mass flux given in Table 8.1.3-1 is actually the mass flux in the steady condition prior to the start of the test. Therefore, the mass flux should not be consistent with the flooding velocity, which is related to the flow during the test. Tests P and Q have similar initial conditions, but the flooding velocities vary significantly. Table 8.1.3-1 will be revised to eliminate any confusion as mentioned in the MHI response to REQUEST 8.1.3-2.

References

1. C. R. Hyman et al., Experimental Investigations of Bundle Boiloff and Reflood under High-Pressure Low Heat Flux Conditions, NUREG/CR-2455, ORNL-5846, 1982.

**REQUEST 8.1.3-4**

Explain how the inlet temperatures of Figure 8.1.3-3 and 8.1.3-6 were selected and compare them with the inlet temperature to the core during the reflood period in a typical SBLOCA transient.

**RESPONSE**

The inlet temperatures of Figures 8.1.3-3 and 6 of MUAP-07013-P (R0) are parameters used in M-RELAP5 analyses as boundary conditions. The data were measured in the test facility (TE-256 in Figure 8.1.2-1 of MUAP-07013-P (R0)), and are compared with the boundary conditions used in Figures 8.1.3-3 and 6 of MUAP-07013-P (R0).

Figure RAI-8.1.3-4.1 shows a comparison between the experimental temperature data and US-APWR SBLOCA temperature range which is derived from the design control document (Ref.1) and the topical report in terms of the SBLOCA sensitivity study (Ref.2). The US-APWR SBLOCA temperature range is specifically determined from 1-in cold leg break to 1-ft<sup>2</sup> cold leg break, which covers the temperature range possible under all the US-APWR SBLOCAs.

Flooding phenomena to quench the dryout fuel cladding mainly occur under the 'recovery' phase, where the temperature varies from 405K to 560K (270-550°F) in the US-APWR SBLOCA. US-APWR, in particular, tends to generate the severest peak cladding temperature (PCT) for the larger break sizes, because the high-head injection system (HHIS) is able to provide the primary reactor coolant system with water sufficient for the smaller break sizes. Therefore, the limiting PCT occurs in the 1-ft<sup>2</sup> break accident when the reactor pressure is about 1MPa (145psia) and the core inlet coolant temperature is about 405K (270°F).

In the THTF reflood tests used for the M-RELAP5 assessment, however, the pressure and inlet coolant temperature are limited to about 4MPa (580psia) and 460K (370°F), respectively. In order to demonstrate that M-RELAP5 is sufficiently applicable to the wider pressure and temperature conditions, MHI is planning to provide an additional verification [

].

It is noted that each phase referred to in Figure RAI-8.1.3-4.1 is defined in the response to REQUEST 4-1.

References

1. MHI, Design Control Document for US-APWR, Chapter 15 Transient and Accident Analyses, MUAP-DC015 Revision 0, December 2007.
2. MHI. Small Break LOCA Sensitivity Analyses for US-APWR, MUAP-07025-P (R0), December 2007.



Figure RAI-8.1.3-4.1 Comparison of Core Inlet Temperature Data with US-APWR/SBLOCA

---

**REQUEST 8.1.3-5**

The inlet temperature profiles for Test P (Figure 8.1.3-3) and Test Q (Figure 8.1.3-6) are substantially different. Explain.

**RESPONSE**

The difference in the temperature evolutions between Tests P and Q was due to the experimental procedure employed for each test. As shown in Figure 8.1.2-1 of MUAP-07013-P (R0), there were two water-feeding lines connected to the test section inlet, the 1/2-in. steady-state inlet flow line and the 3/4-in. reflood line, in the THTF apparatus. The temperatures in Figures 8.1.3-3 and 6 are the mixture mean temperatures of the fluid from these two lines. The initial steady-state condition was attained by adjusting the flow rate through the 1/2-in. line, while the 3/4-in. reflood line was isolated. The transient was activated by feeding additional water from the 3/4-in. reflood line. Because the initially isolated water in the reflood line was cooler than that circulating through the steady-state line, the coolant temperature at the test section inlet temporarily decreased in the beginning of the transient tests as shown in Test P (Figure 8.1.3-3).

For Test Q, on the other hand, the transient flow was sufficiently manipulated by controlling the flow rate through the 1/2-in. steady-state line only. Therefore, no cooler water was supplied to the test section, nor significant transient occurred in the temperature evolution at the test section inlet as shown in Figure 8.1.3-6.

The above is described in the test report (Ref.1).

**References**

1. C. R. Hyman et al., Experimental Investigations of Bundle Boiloff and Reflood under High-Pressure Low Heat Flux Conditions, NUREG/CR-2455, ORNL-5846, 1982.

**REQUEST 8.1.3-6**

Explain how the pressures (boundary condition) in Figures 8.1.3-4 and -7 were selected.

**RESPONSE**

The pressures were measured at the test section outlet (PE-201 in Figure 8.1.2-1), and were used as boundary conditions for the M-RELAP5 calculations, which are compared with the measurements in Figures 8.1.3-4 and 7 of MUAP-07013-P (R0).

Figure RAI-8.1.3-6.1 shows a comparison between the experimental pressure data and the US-APWR SBLOCA pressure range which is derived from the design control document (Ref.1) and the topical report in terms of the SBLOCA sensitivity study (Ref.2).

As discussed in the response to REQUEST 8.1.3-4, the limiting peak cladding temperature (PCT) occurs in the 1-ft<sup>2</sup> break accident when the reactor pressure is just about 1MPa (145psia). THTF tests used for the M-RELAP5 assessment, however, are limited to about 4MPa (580psia) which corresponds to the pressure occurring in the 'recovery' phase of the 5 to 11-in break accidents. Therefore, MHI is planning to provide an additional verification using [ ] .

It is noted that each phase referred to in Figure RAI-8.1.3-6.1 is defined in the response to REQUEST 4-1.

References

1. MHI, Design Control Document for US-APWR, Chapter 15 Transient and Accident Analyses, MUAP-DC015 Revision 0, December 2007.
2. MHI. Small Break LOCA Sensitivity Analyses for US-APWR, MUAP-07025-P (R0), December 2007.

( )



Figure RAI-8.1.3-6.1 Comparison of Pressure Data with US-APWR/SBLOCA

### **REQUEST 8.1.3-8**

The quench velocities for test P (Figure 8.1.3-11) and test Q (Figure 8.1.3.15) are similar for the tests (about 3 cm/sec for P and 2.8 cm/sec for Q), but they are substantially different for the simulations (about 2.4 for P and 1.3 for Q). This may imply that the quench velocities for the simulation could be higher than the test for some parameter ranges, and thus the simulation may not be conservative. Please explain.

### **RESPONSE**

The test report (Ref.1) describes that the average quench rate for Tests P and Q were 3.28cm/s and 2.78cm/s in the experiment, respectively. This difference was due to the difference in the flooding rate, 9.2cm/s for Test P and 5.9cm/s for Test Q. In addition, the test report pointed out that the dominant heat transfer mode around the quench front affected the quench rate, from investigations to dynamic behavior of the measured histories in terms of quench and collapsed levels as follow.

When the quench level is significantly above the collapsed liquid level, dispersed flow film boiling is suggested, while the inverted annular film boiling may be suggested when the quench level is near or below the collapsed level. These heat transfer and hydraulic flow regimes are schematically compared in Figure RAI-8.1.3-8.1 (Ref.2). Next, Figures RAI-8.1.3-8.2 and 3 show comparisons between the measured quench level and collapsed level histories for Tests P and Q, respectively, indicating that the dispersed flow film boiling possibly appeared in Test Q rather than Test P. Under the dispersed flow film boiling like Test Q, numerous droplets occur from the liquid level front, which effectively contribute to the precursor cooling above the liquid level before quench. This effectively decreases the vapor superheat and the fuel rod surface temperature in the uncovered-bundle region, and thus hastens the quench rate even though the flooding rate is low. This is why the difference in the measured quench rates between Tests P and Q was relatively small, in spite of the fact that the flooding rates were significantly different from each other.

On the other hand, the average quench rates by M-RELAP5 are [ ] for Tests P and Q, respectively. The ratio of quench-to-flooding rate is smaller in the lower flooding case (Test Q) for M-RELAP5 in contrast to the measurements, as arranged in Table RAI-8.1.3-8.1. This tendency in the M-RELAP5 prediction can be explained by modeling for the precursor cooling effect, namely by the wall heat transfer model applicable to the uncovered-bundle region in M-RELAP5. M-RELAP5 does not model an explicit droplet field and therefore does not represent the cooling effect of droplets on the heated wall and vapor just above the mixture-level. Hence, the wall heat transfer under the dispersed flow film boiling (Test Q) is conservatively represented by the vapor convection (single-phase vapor), while the inverted flow film boiling (Test P) is reasonably modeled by the Bromley heat transfer correlation.

Figures RAI-8.1.3-8.4 and 5 show comparisons between the collapsed and quench levels calculated by M-RELAP5 for Tests P and Q, respectively. The precursor cooling effect predicted by M-RELAP5 is significantly less than the measurement for Test Q. Figures RAI-8.1.3-8.6 and 7 show the axial distributions in terms of the applied heat transfer mode and computed heat transfer coefficient by M-RELAP5 for Tests P and Q, respectively. It is found that the dryout heat transfer coefficient just above the quench front in Test Q is reduced to [ ], due to the heat transfer mode different from Test P.

This possibly induces that the predicted precursor cooling effect is conservatively underestimated in Test Q rather than in Test P, resulting in underestimation of quench rate in Test Q.

Regarding the inverted flow film boiling regime, M-RELAP5 evaluates its heat transfer coefficient by the Bromley correlation. Because the Bromley correlation describes the heat transfer from the heated wall to the stagnant and non-contact liquid fluid without the turbulent convection effect, the correlation tends to underestimate the heat transfer coefficient with increase in the fluid Reynolds number. This indicates that M-RELAP5 tends to underestimate the heat transfer in the inverted flow film boiling regime under the relatively high flow condition.

In conclusion, M-RELAP5 theoretically tends to underestimate the heat transfer coefficient both for the low flow/dispersed flow film boiling and for the high flow/inverted flow film boiling, and to predict slower quench rates in comparison to the measurements as confirmed by Table RAI-8.1.3-8.1. Finally, it is noted that the code applicability to the wide pressure range, i.e. various break sizes, is to be verified using the additional [ ] IET data.

References

1. C. R. Hyman et al., Experimental Investigations of Bundle Boiloff and Reflood under High-Pressure Low Heat Flux Conditions, NUREG/CR-2455, ORNL-5846, 1982.
2. USNRC, Compendium of ECCS Research for Realistic LOCA Analysis, NUREG-1230 Revision 4, 1988.

Table RAI-8.1.3-8.1 Comparison between Measured and Calculated Quench Rate

Test	Initial pressure (MPa)	Linear heat rate (kW/m)	Average flooding rate (cm/s)	Meas. average quench rate (cm/s)	Cal. average quench rate (cm/s)
3.09.10P	4.28	1.00	9.2	3.28	
				(0.36)*	
3.09.10Q	3.95	1.02	5.9	2.78	
				(0.47)*	

\*Ratio of quench-to-flooding rate

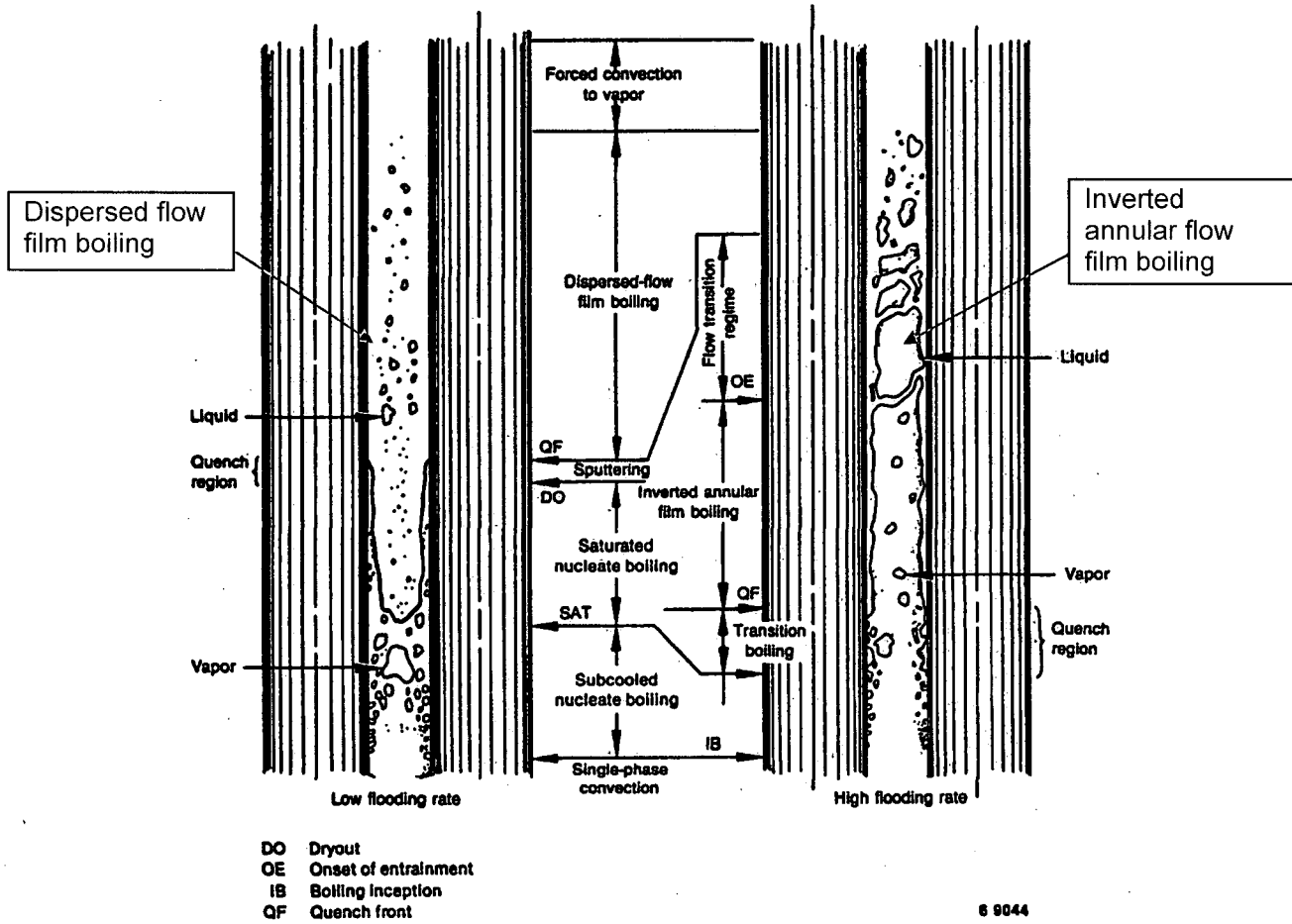


Figure 6.4-3. Heat transfer and hydraulic flow regimes for bottom reflow.

Figure RAI-8.1.3-8.1 Heat Transfer and Hydraulic Flow Regimes for Bottom Reflood (Ref.2)

ORNL-DWG 81-20399 ETD

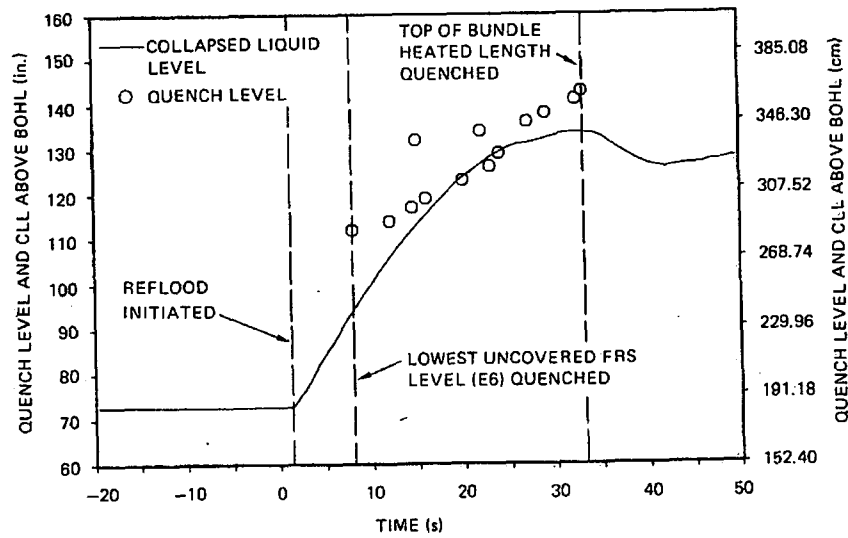


Fig. 72. Quench level and collapsed liquid level histories, test 3.09.10P.

Figure RAI-8.1.3-8.2 Measured Quench Level and Collapsed Liquid Level Histories (Test 3.09.10P)

ORNL-DWG 81-20400 ETD

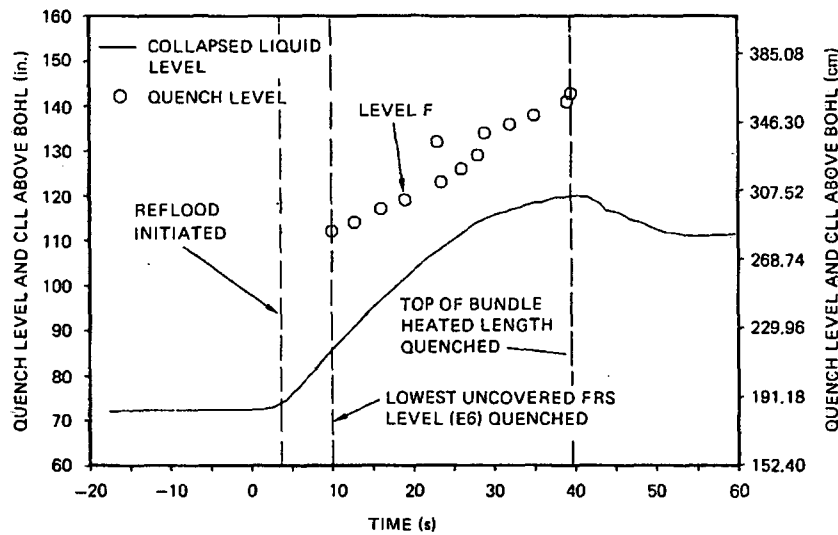


Fig. 73. Quench level and collapsed liquid level histories, test 3.09.10Q.

Figure RAI-8.1.3-8.3 Measured Quench Level and Collapsed Liquid Level Histories (Test 3.09.10Q)

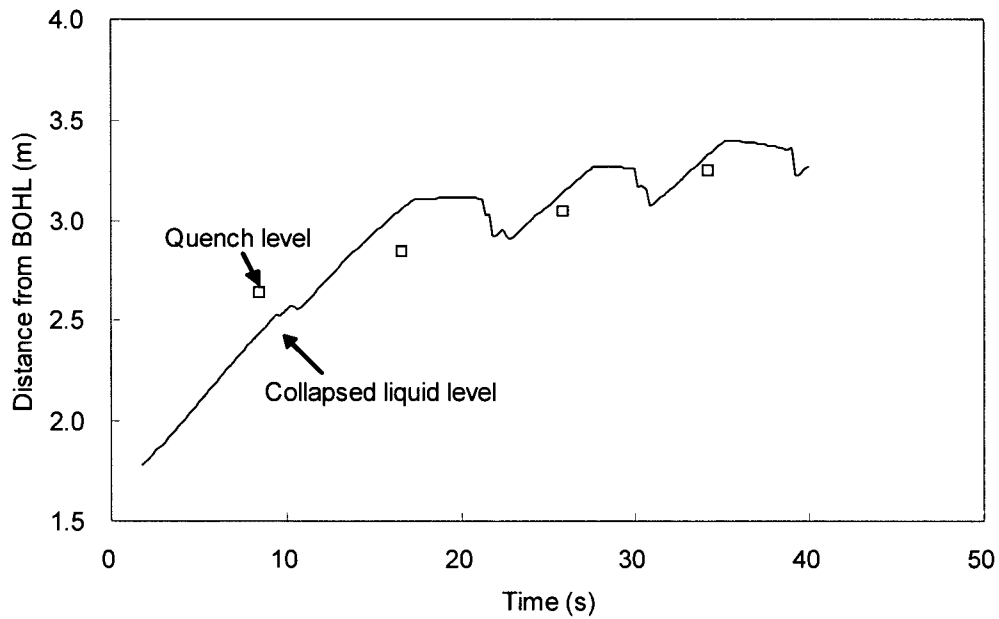


Figure RAI-8.1.3-8.4 Calculated Quench Level and Collapsed Liquid Level Histories (Test 3.09.10P)

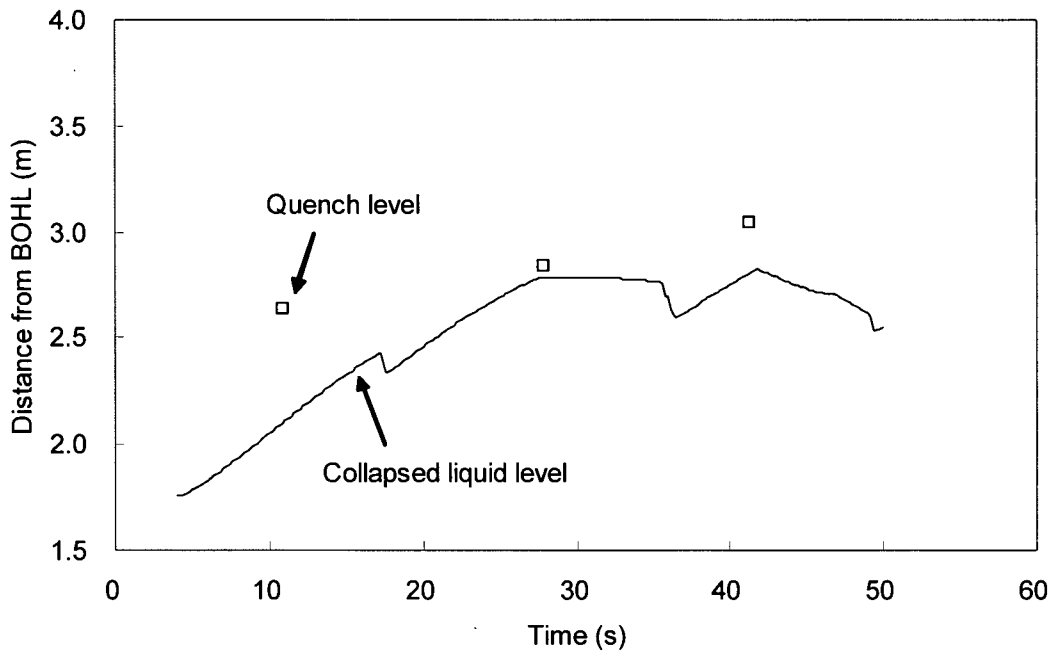


Figure RAI-8.1.3-8.5 Calculated Quench Level and Collapsed Liquid Level Histories (Test 3.09.10Q)



Figure RAI-8.1.3-8.6 Comparison of M-RELAP5 HTMODE between Tests P and Q



Figure RAI-8.1.3-8.7 Comparison of M-RELAP5 HTC between Tests P and Q

**REQUEST 8.1.4-1**

The UPTF test description mentions steam injection and air injection (Section 8.1.4.2). Is it correct? Was the test steam only?

**RESPONSE**

Injected gas phase in the UPTF test was steam only and the description of "air" injection is incorrect. The term will be revised from air to steam.

**REQUEST 8.1.4-2**

[Empty response box for Request 8.1.4-2]

**RESPONSE**

[Empty response box for Response]

### **REQUEST 8.1.4-3**

RELAP5 uses CCFL correlation with three input specified parameters that indicates the effect of surface tension and gas flow rate for hold up. It correctly indicates that for large pipes surface tension is important (Kutateladze correlation) and for small pipes the length scale does not depend on surface tension.

However, there is no statement on size of the pipe where the transition occurs. Explain the criteria for selecting the use of either the "big" pipe or "small" pipe form of the CCFL correlation.

### **RESPONSE**

The criteria could be judged between the big and small pipes based on Fig.2 in Ref.1 (shown in Figure RAI-8.1.4-3.1) and Fig.25 in Ref.2. As shown in Figure RAI-8.1.4-3.1, Kutateladze number (depending on steam flow rate) giving zero penetration of water increases with  $D^* : (D \cdot (g(\rho_L - \rho_G)/\sigma)^{1/2})$  and approaches to a constant value which is about 3.2 for  $D^*$  greater than about 60. The value of  $D$  at  $D^*=60$  was derived as a function of pressure as shown in Table RAI-8.1.4-3.1. From this table, the Ku correlation was applied to the hot leg nozzle of the steam generator inlet plenum and was applied the correlation using hydraulic-equivalent diameter as the length-scale to the inlet of the tubes in the steam generators.

#### References

1. Richter, H.J., Flooding in tubes and annuli, Int. J. Multiphase Flow, Vol. 7, No. 6, pp. 647-658, 1981.
2. Bankoff, S.G. and Lee, S.C., A Critical Review of the Flooding Literature, NUREG/CR-3060, 1983.

Table RAI-8.1.4-3.1 Value of D at  $D^*=60$  under different pressure

Pressure (bar)	3	15	70	150
D (in.)	5.5	5.1	3.9	2.4

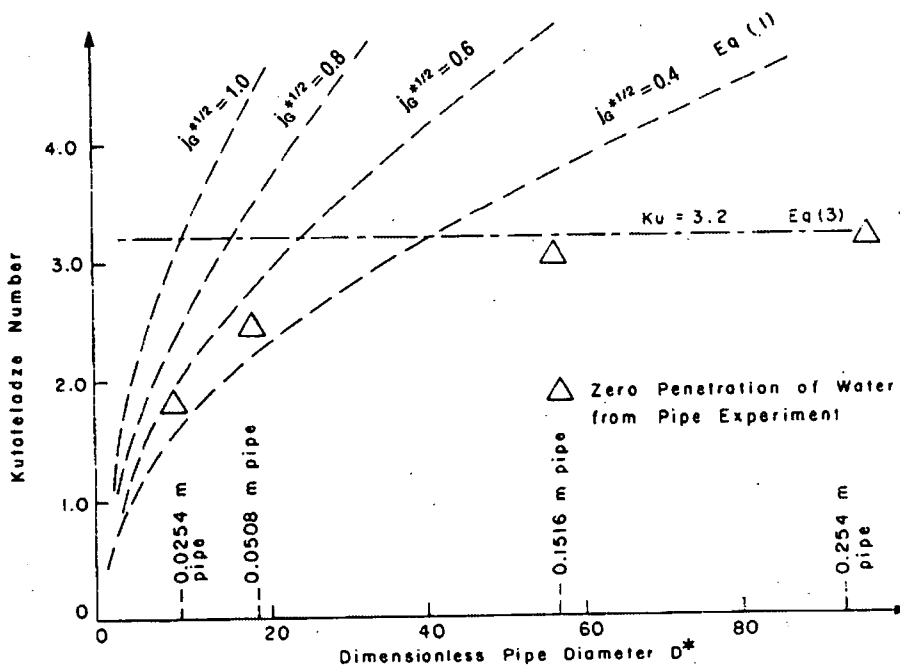


Fig. 2. Kutateladze number vs nondimensional geometric parameter and experimental results for zero penetration of liquid.

Figure RAI-8.1.4-3.1 Kutateladze number vs. nondimensional geometric parameter and experimental results for zero penetration of liquid

**REQUEST 8.1.4-4**

The large pipe CCFL correlation was obtained by regression analyses of the actual UPTF data. The coefficients ( $m$ ,  $c$ ,  $\beta$ ), obtained from these analyses, are used to model these tests with RELAP5 as part of validation. However, this is not a validation but verification of implementation of the model. What set of coefficients will be used in plant simulation?

**RESPONSE**

The same set of coefficients ( $m$ ,  $c$ ,  $\beta$ ),  $\beta=1.0$ ) was applied, which was obtained from the UPTF data in the plant simulations.

**REQUEST 8.1.4-6**

Figure 8.1.4-4 indicates a comparison of code prediction and the test results. Are there code results for actual test conditions? How do they compare? For 3 bar case, there are three steam flow rates with liquid upward flow but none in the data. Please explain.

**RESPONSE**

In the code prediction, the same steam flow rate was not set as in the UPTF test but was instead set the steam flow rate to the values given in Table 8.1.4-1. The liquid downward flow rate was evaluated under each steam flow rate in that table and therefore some different characteristics are recognized in the comparison. The liquid upward flow calculation could be attributed to the relatively large discrepancy between the test results at 3 bar and the regression relation shown in Figure 8.1.4-2.

### **REQUEST 8.1.5-1**

Discuss the scaling of the Dukler Air-Water Flooding test facility in comparison with the US-APWR steam generator tubes (diameter, length, friction factor, etc.),

### **RESPONSE**

The comparison between the Dukler test facility and the US-APWR for the configuration and the fluid combination is shown in Table RAI-8.1.5-1.1. The subject on scaling for each item is considered as follows:

1. Tube diameter: The CCFL in steam generator (SG) tubes focuses on the interaction between the liquid film condensed within the tube and the upward steam flow. This implies less impact of tube end geometry affecting the CCFL curve and then the coefficient set ( $m=1.0$ ,  $c=0.88$ ,  $\beta=0.0$ ) which is recommended in Ref. 5.2.1.6-2 is adopted when end effects are minimized. The  $J^*$  scaling (Eq. 5.2.1.6-4) is considered to have a high adaptability for a small-scale pipe as discussed in the response of REQUEST 8.1.4-3 and the experimental data by Dukler in this section are indeed located near the curve as shown in Figure 8.1.5-4. Figure 5.2.1.6-5 (from Ref. 5.2.1.6-2) indicates that Eq. 5.2.1.6-4 correlates well the data irrespective of the tube diameter 3/4" or 5/4". The tube diameter 3/4" is near the US-APWR and the adaptability of the correlation is considered to be high.
2. Tube length: The phenomena restricting the downward liquid flow rate in SG tubes is considered to be governed by those near the bottom of the tubes where the steam and condensed liquid flows are maximized. The effect of tube length is unlikely to be important under the situation. Figure 5.2.1.6-5 shows several experimental data but the effect of length is not reported to be an affecting parameter.
3. Tube wall material: The effect of wall friction is considered to be smaller than the interfacial friction and any experimental studies on the wall friction against CCFL have not been recognized as far as MHI concerned. The coefficient  $c$  in ROSA-IV/LSTF is shown in the next item (4. Fluid combination) and the value is the same as Eq. 5.2.1.6-4. This means the effect of tube wall material is not significant because the LSTF uses stainless-steel tubes and the Dukler experiment Plexiglas. In the penetration region, the wall friction might have some effect because the water down flow rate in Dukler experiment tends to be larger than Eq. 5.2.1.6-4.
4. Fluid combination: Ref.1 revealed that the difference of fluid combination (air/water vs. steam/water) can be scaled by  $J^*$  parameter (Figure RAI-8.1.5-1.1). Furthermore ROSA-IV/LSTF tests investigated the steam flow rate giving zero water penetration at the bottom of SG tubes (Ref.2) as shown below in Figure RAI-8.1.5-1.2 and the same coefficient  $c=0.88$  was reported. These results support the same coefficient set ( $m=1.0$ ,  $c=0.88$ ,  $\beta=0.0$ ) can apply to the US-APWR analyses.

#### References

1. Ohnuki, A., Experimental study of counter-current two-phase flow in horizontal tube connected to inclined riser, J. Nucl. Sci. Technol., Vol. 23, No. 3, pp 219-232, 1986.
2. Kukita, Y., Anoda, Y. and Tasaka, K., Summary of ROSA-IV LSTF first-phase test program – Integral simulation of PWR small-break LOCAs and transients -, Nucl. Eng. Design, Vol. 131, pp 101-111, 1991.

Table RAI-8.1.5-1.1 Comparison of configuration and fluid combination

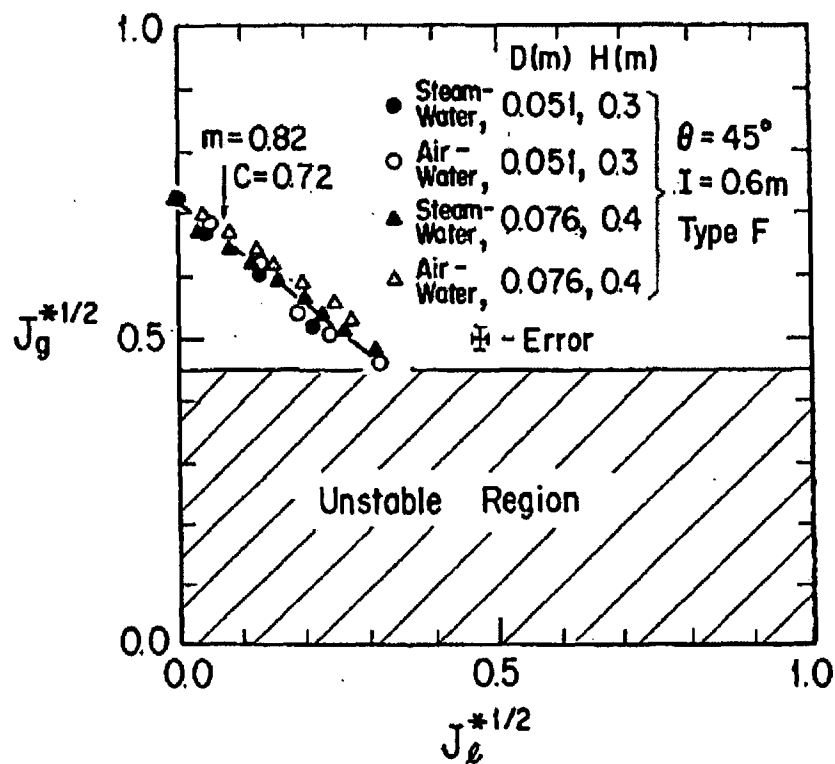


Fig. 8 Effect of fluid combinations (air/water and steam/water)

Figure RAI-8.1.5-1.1 Effect of fluid combinations

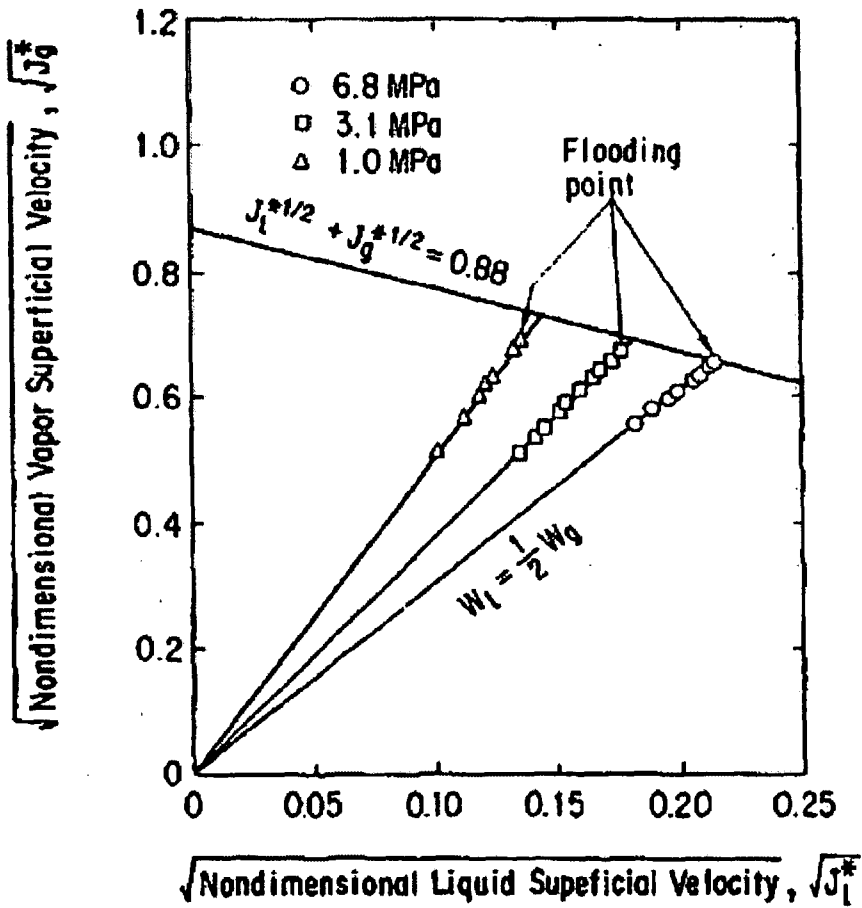


Fig. 13. Steam generator (SG) U-tube CCFL characteristics.

Figure RAI-8.1.5-1.2 SG U-tube CCFL characteristics in ROSA-IV/LSTF

**REQUEST 8.1.5-2**

Compare the test pressure, temperature and flow rates (both water and air) with those of the expected conditions at the SG U-tube uphill side during the loop seal clearing period, and discuss why these tests are applicable to the loop seal period of a SBLOCA.

**RESPONSE**

As investigated in the response of REQUEST 8.1.5-1, the CCFL correlation Eq. 5.2.1.6-4 using  $J^*$  parameter has a high potential to scale the difference of the configuration and the fluid combination between the Dukler test facility and the US-APWR. Furthermore, the CCFL correlation gives an important contribution during the loop seal clearing period. Figure RAI-8.1.5-2.1 shows the transients of  $J^*$  at intact loop side SG tubes in the ROSA-IV/LSTF analysis (Section 8.2). The comparison with the CCFL correlation is also included. The CCFL governs the down flow rate in the period of LS (Loop Seal) formation-clearance until the time of clearing.



Figure RAI-8.1.5-2.1  $J^*$  at intact loop side SG tube in the ROSA-IV/LSTF analysis and comparison with CCFL correlation

**REQUEST 8.1.5-3**

The test sections are made of Plexiglas/flexible tygon tubing while the SG tubes are made of inconel. Discuss the impact of the pipe material difference in assessing the applicability of the test results, since the surface property (friction factor and surface tension) of the pipes may influence the results. Smooth surface may be more inductive to more water going down, which the results indicate.

**RESPONSE**

The response on this subject is stated at the response-3 in REQUEST 8.1.5-1.

**REQUEST 8.1.5-4**

The test was performed with water and non-condensable gas (air), while the fluid in the SG tubes is condensable water/steam mixture during SBLOCA. Discuss the applicability of this test in spite of this difference.

**RESPONSE**

The response on this subject is stated at the response-4 in REQUEST 8.1.5-1.

---

**REQUEST 8.1.5-5**

Discuss if the test cover all flow regimes since reflood/reflux flow would be affected by the flow regime.

**RESPONSE**

In the Dukler flooding test, annular countercurrent flow was mainly investigated and a slugging flow was reported under a low air upward flow rate after flooding occurred. Basically, the same flow regime is predicted in M-RELAP5 analyses although the predictive accuracy on the flow regime boundary is not clear due to lack of experimental information especially on the axial variation of flow regime. The amount of liquid accumulation within the uphill side of SG U-tubes is one of most important values affecting the core liquid level. The CCFL characteristics and the flow regime predictions affect the value. The former subject is investigated in this section and Eq. 5.2.1.6-4 is confirmed to have a high potential to apply to the actual conditions as stated in the responses in REQUEST 8.1.5-1 and 8.1.5-2. The latter one (flow regime predictions) is indirectly evaluated in section 8.2.1 ROSA-IV/LSTF analysis through comparisons of differential pressures along the uphill side of SG U-tubes. Reasonable agreements were obtained on the differential pressure shown in Figure 8.2.1-26 and 8.2.1-27. The high adaptability of Eq. 5.2.1.6-4 and the good predictions for the differential pressures indicate no significant problems due to flow regime predictions.

**REQUEST 8.1.5-6**

Is the CCFL correlation described in Section 8.1.5.3.b, namely the three parameters in the Hewitt & Wallis correlation, the same one used in all SBLOCA simulations?

**RESPONSE**

The same parameters were used in all SBLOCA simulations.

### **REQUEST 8.2.1-1**

The assessment of M-RELAP5 against the ROSA-IV/LSTF tests was for application to the US-APWR. Table 8.2.1-1 showed the scaling of the major design characteristics of the test facility against a PWR. Provide a similar table for the US-APWR.

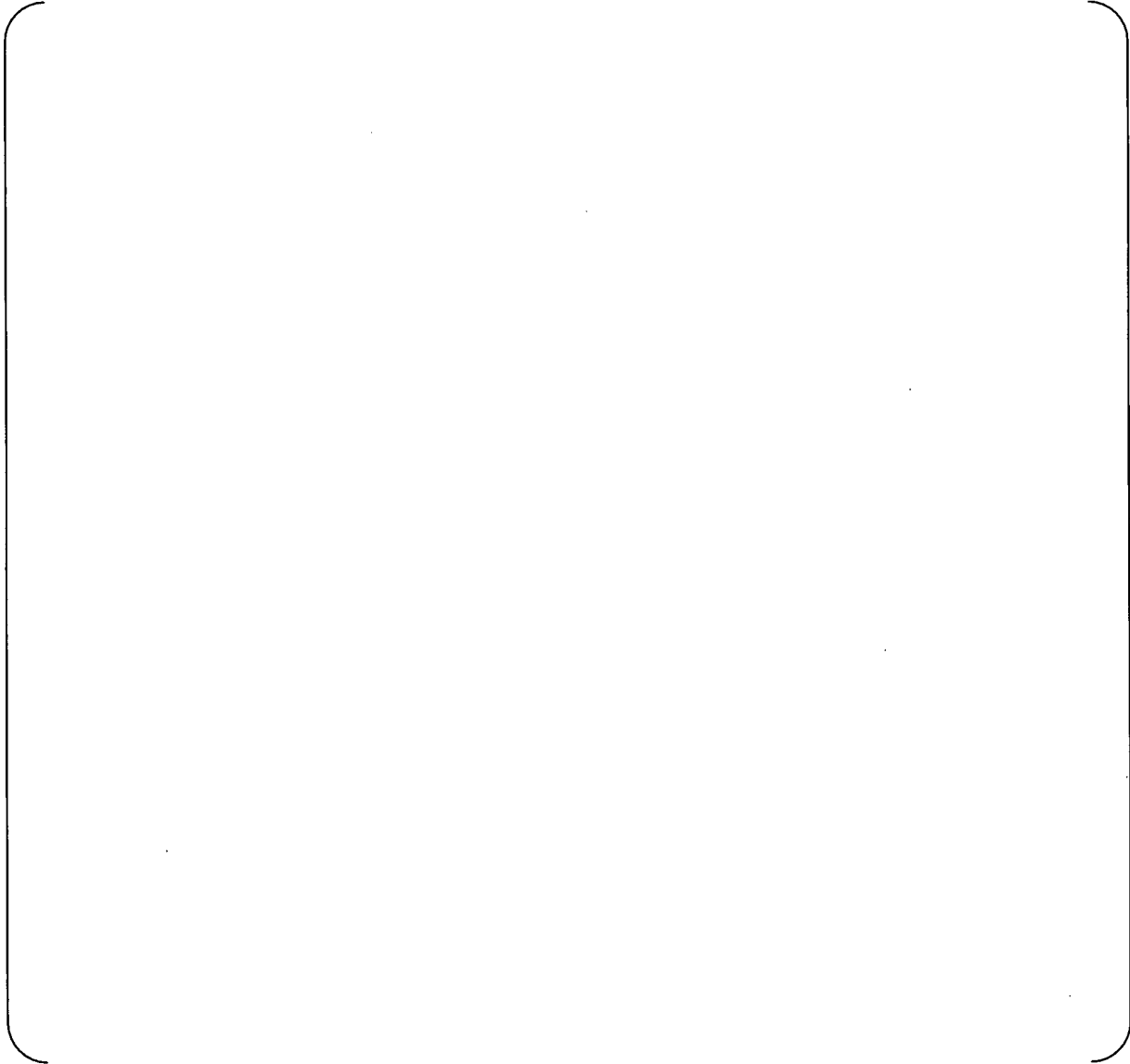
### **RESPONSE**

Table RAI-8.2.1-1.1 shows the scaling of the major design characteristics of the test facility against a US-APWR and a PWR. The scaling between the test facility and the US-APWR is similar to that between the test facility and a PWR.

#### References

1. The ROSA-IV Group, ROSA-IV Large Scale Test Facility (LSTF) System Description, JAERI-M84-237, 1985.
2. Kumamaru, H., et al., ROSA-IV/LSTF 5% Cold Leg Break LOCA Experiment RUN SB-CL-18 Data Report, JAERI-M89-113.

Table RAI-8.2.1-1.1 Major Design Characteristics of LSTF and PWR

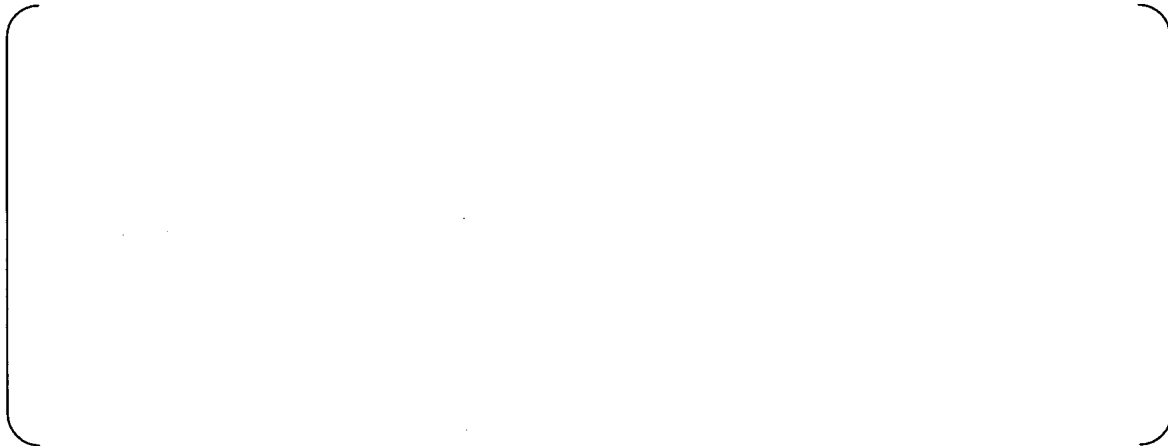


**REQUEST 8.2.1-2**

In Section 8.2.1.3 (a), it was stated that "the hot and cold legs were sized to conserve the volume scaling and ratio of the length to the square root of pipe diameter,  $L/\sqrt{D}$ , for the reference PWR." Does this still hold for the US-APWR? If not, discuss the implication or why this does not matter,

**RESPONSE**

The volume scaling and ratio of the length to the square root of pipe diameter,  $L/\sqrt{D}$  are shown in Table RAI-8.2.1-1.1. MHI judged that the parameter scaling between LSTF and US-APWR does not cause any concern. The reason is as follows;



**References**

1. N. Zuber, Problems in Modeling of Small Break LOCA, NUREG-0724, 1980.

---

**REQUEST 8.2.1-4**

What is the timing of 10 MW in the decay heat curve (120% of ANS curve) in terms of scaling with respect to the US-APWR?

**RESPONSE**

The power curve of ROSA-IV assumes that the initial power is 71.3MW (see Footnote 2 of Table RAI-8.2.1-1.1). 10MW is about 14% of 71.3MW, which exceeds 120% of the initial value of decay heat from the ANS curve. The ROSA-IV power curve is higher because it simulates delayed neutron fission power following reactor trip. The time after initiation of control rod insertion that the core power reaches 14% of the initial power follows for the US-APWR analysis:

1-ft <sup>2</sup> break	:	about 4 seconds
7.5-inch break	:	about 9 seconds
2-inch break	:	about 11 seconds

The time depends on the break size because of the reactivity feedback.

References

1. MHI, Small Break LOCA Sensitivity Analyses for US-APWR, MUAP-07025-P (R0), December 2007.

**REQUEST 8.2.1-5**



**RESPONSE**



